

Constraint on scalar leptoquark from low energy leptonic observables

Uladzimir Khasianeovich,^{*} Dominik Stöckinger,[†]
Hyejung Stöckinger-Kim,[‡] and Johannes Wünsche[§]
*Institut für Kern- und Teilchenphysik, TU Dresden,
Zellescher Weg 19, 01069 Dresden, Germany*

arXiv:2305.05016v2 [hep-ph] 30 Oct 2023

Abstract

We consider the flavor structure of the S_1 leptoquark model and derive conservative constraints on the elements of the left- and right-handed coupling matrices in a number of representative scenarios. We focus on the cases where the muon $g-2$ deviation is explained by real muon couplings to either the top-quark or to the charm-quark or to all up-type quarks. The most significant constraints arise from charged lepton flavor violating decays of the muon and the τ lepton and from the $\mu-e$ conversion process. Kaon decays and perturbativity provide further constraints. We find strong constraints on almost all coupling matrix elements, implying a very hierarchical matrix structure, where individual entries must differ by at least 4 orders of magnitude. The `FlexibleSUSY` program was used with appropriate model files incorporating the parameterization of the couplings in the up-type mass diagonal basis. The expressions for the leptonic observables were generated and cross-checked with the help of the `NPointFunctions` extension of the `FlexibleSUSY` program.

CONTENTS

I. Introduction	3
II. Model definition	5
III. Analytical results	6
A. Δa_μ	7
B. $\ell_i \rightarrow \ell_j \gamma$	9
C. $\ell_i \rightarrow \ell_j \ell_k \ell_k^c$	9
D. $\mu \rightarrow e$ conversion	12
IV. Analysis strategy	13
V. Phenomenological consequences of Δa_μ	15
VI. Phenomenological consequences of two-body decays $\mu \rightarrow e \gamma$, $\tau \rightarrow e \gamma$, and $\tau \rightarrow \mu \gamma$	19
A. Consequences of decays involving muons	19

* uladzimir.khasianeveich@tu-dresden.de

† dominik.stoeckinger@tu-dresden.de

‡ hyejung.stoeckinger-kim@tu-dresden.de

§ johannes.wuensche@tu-dresden.de

B. Consequences for $\tau \rightarrow e\gamma$	23
VII. Phenomenological consequences of three-body decays $\mu \rightarrow 3e$ and others	23
VIII. Phenomenological consequences of $\mu \rightarrow e$ conversion	27
IX. Conclusions	29
Acknowledgments	31
A. Constraints from flavor-conserving meson decays	31
1. Decay $K^+ \rightarrow \pi^+ \nu \bar{\nu}$	31
2. Decay $D^0 \rightarrow \mu^+ \mu^-$	33
References	33

I. INTRODUCTION

Low-energy lepton precision physics provides an excellent probe of fundamental interactions with the potential of discovering new physics beyond the Standard Model (SM) and shedding light on the origin of mass and flavor. The anomalous magnetic moment of the muon a_μ is a flavor- and CP-conserving observable which corresponds to a chirality-flipping dipole operator. There is a longstanding discrepancy between the experimental determination at the BNL and Fermilab measurements and the SM theory prediction:¹

$$\Delta a_\mu^{2021} = a_\mu^{\text{Exp, 2021}} - a_\mu^{\text{SM}} = (25.1 \pm 5.9) \cdot 10^{-10}. \quad (1)$$

This value is based on the Fermilab Run-1 result [2], the Brookhaven result [3], and the Standard Model White Paper [4], which itself uses results from original references [5–30]. After the White Paper [4], several lattice gauge theory results [31–34] and the CMD-3 measurement [35] of $e^+e^- \rightarrow$ hadrons are in tension with earlier results and tend to prefer higher values of the hadronic vacuum polarization contributions to a_μ . Taking those results at face value would reduce Δa_μ^{2021} to about half its quoted value, but scrutiny of these

¹ Since the release of this paper there has been an update on the experimental average of the anomalous magnetic moment of the muon from Run-2 of the FNAL experiment Δa_μ^{2023} , see Ref. [1]. This paper represents the measurement from before this latest update.

results is ongoing, and further progress on the hadronic vacuum polarization contributions is expected in the coming years [36]. Furthermore, more precise experimental determinations of Δa_μ based on Run-2/3 data and later on Run-4/5/6 data from the Fermilab experiment are in preparation. In view of this progress it remains relevant to ask which scenarios for physics beyond the SM could explain a deviation as large as Eq. (1) without violating other existing constraints.

A very promising way to explain the deviation Δa_μ is via scenarios beyond the SM (BSM) with enhanced chirality flips. Such scenarios are also interesting from the point of view of electroweak symmetry breaking as they necessarily contribute to the fermion mass generation mechanism and to effective Higgs-boson couplings [37–40]. At the same time, there is currently no sign of new physics in searches for charged lepton flavor violation (CLFV), despite the potential of correlations of BSM effects on Δa_μ and CLFV observables in many concrete models. Typically, therefore, such models can only explain the deviation (1) in non-generic parameter regions with large hierarchies between flavor-conserving and flavor-violating parameters. Here we study this conflict between Δa_μ and CLFV in a concrete model, using the value of (1) as an illustration. The conclusions of the present paper would essentially remain intact even if the deviation would reduce to a smaller value.

Leptoquark (LQ) models are among the best-motivated extensions of the SM. Using the notation of Ref. [41], there are two possible types of spin-0 LQ quantum numbers, S_1 and R_2 , which allow gauge invariant couplings to both left-handed and right-handed leptons. These, therefore, allow enhanced chirality flips and promising explanations of Δa_μ [42–55]. More generally, the S_1 and R_2 models are two of very few viable single-field explanations of Δa_μ [37, 45, 56–58]. In the past years, LQ models have also frequently been proposed as combined explanations of B -physics anomalies and Δa_μ [46–48, 59–65], and models with several leptoquarks are also able to simultaneously explain neutrino masses [47, 61, 65]. Refs. [49, 52, 55] confirm that the single LQ explanations of Δa_μ remain viable also given constraints on LQs from Z-boson and Higgs-boson decays.

The S_1 and R_2 LQ models exemplify how large, chirality-flip enhanced contributions to Δa_μ can naturally be accompanied by CLFV effects. Focusing on the S_1 model, its flavor structure is governed by two 3×3 coupling matrices, i.e. by 18 free parameters $\lambda_{L,R}^{q\ell}$ coupling left- or right-handed quarks q to leptons ℓ . Δa_μ depends on couplings of the muon to the top- or charm-quark, while non-zero couplings of the electron and τ lepton can lead to CLFV

contributions.

Here we focus on the impact of CLFV versus Δa_μ constraints on the flavor structure of the S_1 LQ model. We aim for deriving general constraints on the 18 flavor parameters, under the assumption that the model explains Δa_μ . To keep the analysis concrete, we consider several representative scenarios for the flavor structure which we call top-only, charm-only and up-type quark universal, as specified further in Sec. IV. Our study is complementary to Ref. [65], where Δa_μ , neutrino masses and complementary observables were fitted to a minimal LQ model (containing S_1 and further particles and general flavor coupling structure), leading to specific best-fit values for the flavor parameters of the model. It is also complementary to Refs. [66, 67], where upper limits on flavor parameters were derived without requiring an explanation of the nonzero result for Δa_μ . In our case, the S_1 model alone cannot explain neutrino masses; we aim for conservative and general limits on the flavor parameters under the assumption that leptoquarks are responsible for Δa_μ . The limits will be derived from correlations between Δa_μ and various lepton flavor violation processes, such as two-body decays $\ell_i \rightarrow \ell_j \gamma$, three-body decays $\ell_i \rightarrow \ell_j \ell_k \ell_k^c$, and $\mu - e$ conversion in nuclei processes, as $\mu Au \rightarrow e Au$ and $\mu Al \rightarrow e Al$. To manage a large number of free parameters, we restrict ourselves to several specific cases, where the anomalous magnetic moment of muon is explained either only by the top-quark or by charm-quark contributions or by a combination thereof.

The paper is structured as follows. In Sec. II we introduce our notations for the S_1 leptoquark model, and Sec. III with the appendix present the relevant analytical expressions of the considered observables. Later, in Sec. IV the latest constraints on the leptoquark mass from the LHC studies are shown and our analysis strategy is explained. In Secs. V–VIII we show analytical results for observables under interest and derive the constraints on coupling constants that induce them. Finally, the most important results are combined as conclusions in Sec. IX.

II. MODEL DEFINITION

We consider the leptoquark S_1 model, which extends the SM particle content by a single spin-0 leptoquark field with the gauge representation $(\bar{\mathbf{3}}, \mathbf{1}, 1/3)$ under the $SU(3) \times SU(2) \times U(1)$ group. The leptoquark is an $SU(2)$ singlet thus carrying an electric charge of $Q_{S_1} =$

1/3. The Lagrangian terms involving the S_1 leptoquark which are relevant for this study are expressed in the following way in the *interaction* eigenstate basis (indicated by a tilde),

$$\mathcal{L} \ni -m_{S_1}^2 |S_1|^2 - \left(\tilde{\lambda}_L^{ql} \overline{\tilde{Q}}_q^c i \sigma_2 \tilde{L}_l S_1 + \tilde{\lambda}_R^{ql} \overline{\tilde{u}}_q^{Rc} \tilde{e}_l^R S_1 + h.c. \right), \quad (2)$$

containing the $SU(2)$ -invariant product of the left-chiral quark and charged lepton doublet fields,

$$\overline{\tilde{Q}}_q^c i \sigma_2 \tilde{L}_l = \overline{\tilde{u}}_q^{Lc} \tilde{e}_l^L - \overline{\tilde{d}}_q^{Lc} \nu_l^L. \quad (3)$$

This fermion-leptoquark interaction Lagrangian is the most general one for the S_1 leptoquark type which prevents fast proton decay by excluding couplings to quark-antiquark pairs.

For studying flavor physics, it is useful to rotate the fermion fields into mass eigenstates. To perform this, the unitary matrices $U_{u,d,e}$, $V_{u,d,e}$ for left- and right-handed fermion fields are applied (schematically as $\tilde{\psi}_k = U_{ik}^* \psi_i^{mass} \equiv U_{ik}^* \psi_i$).

In this way, the Standard Model Yukawa couplings and fermion mass terms are diagonalized. The mixing matrices can be fully absorbed in two out of the three leptoquark interaction terms with left-/right-handed leptons and neutrinos. We choose the so-called *up-type mass diagonal basis* [68, 69], where the new leptoquark coupling matrices are defined as

$$\lambda_L^{ql} = V_u^{\dagger iq} \tilde{\lambda}_L^{ij} V_e^{\dagger jl}, \quad \lambda_R^{ql} = U_d^{\dagger iq} \tilde{\lambda}_L^{ij} U_e^{\dagger jl}. \quad (4)$$

Using these couplings the interaction Lagrangian contains interactions with charged leptons and up-type quarks governed directly by the $\lambda_{L,R}$, while the interaction with neutrinos and down-type quarks involves the CKM matrix V_{CKM} ,

$$\mathcal{L} \ni -\overline{u}_q^c (\lambda_L^{ql} P_L + \lambda_R^{ql} P_R) e_l S_1 + \overline{d}_q^c (\lambda_L^{jl} V_{CKM}^{jq} P_L) \nu_l S_1 + h.c. \quad (5)$$

As numerical values for the CKM matrix entries, we use the ones by the PDG [70].

III. ANALYTICAL RESULTS

In the present paper, we consider low-energy lepton observables as constraints on the S_1 leptoquark model. The observables are the muon magnetic moment $a_\mu = (g - 2)_\mu/2$, two-body decays $\ell_i \rightarrow \ell_j \gamma$, three-body decays of the form $\ell_i \rightarrow \ell_j \ell_k \ell_k^c$, and $\mu \rightarrow e$ conversion in the presence of a nucleus. Table I summarizes these observables, current experimental

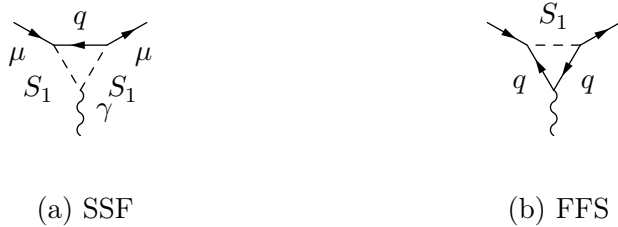


FIG. 1: One-loop diagrams contributing to Δa_μ induced by S_1 leptoquark.

limits, and expected sensitivities of the next planned experiments. The present section collects analytical results for the leptoquark contributions to all these observables. Additional observables involving meson decays are discussed in the appendix.

All one-loop results were obtained in two ways. First, by direct Feynman diagrammatic calculation. Second, by automatic generation using `FlexibleSUSY` [71–73] and its extension package `NPointFunctions` [74]. `FlexibleSUSY` is a `Mathematica` and `C++` framework which compiles a spectrum generator out of a given model definition input. It uses `SARAH` [75, 76], for which we created a suitable model file incorporating the parameterization of the couplings developed in Sec. II. This setup resulted in an independent cross-check of the consistency of the results presented in the following.

A. Δa_μ

The two relevant one-loop Feynman diagrams contributing to Δa_μ , i.e. the additional leptoquark contribution to a_μ , are depicted in Figure 1. Both diagrams have a very similar structure and involve an up-type quark next to the leptoquark; they are often referred to as SSF (see Figure 1a) and FFS (see Figure 1b), respectively.

Their sum can be written as

$$\Delta a_\mu^{\text{one-loop}} = \frac{m_\mu^2}{48\pi^2 m_{S_1}^2} \left(\frac{m_q}{m_\mu} \lambda_L^{q2} \lambda_R^{q2} L_1(x_q) + \frac{(\lambda_L^{q2})^2 + (\lambda_R^{q2})^2}{4} L_2(x_q) \right), \quad (6)$$

$$\Delta a_\mu = \delta_{\text{QED}} \Delta a_\mu^{\text{one-loop}}, \quad \delta_{\text{QED}} = 1 + \frac{e^2}{\pi^2} \ln \frac{m_\mu}{m_{S_1}},$$

with the shorthand notation of the one-loop mass ratio argument $x_q = m_q^2/m_{S_1}^2$ used here and in the following. This result coincides with the formulas presented e.g. in Ref. [37] (see also references therein) and includes universal leading logarithmic two-loop QED corrections

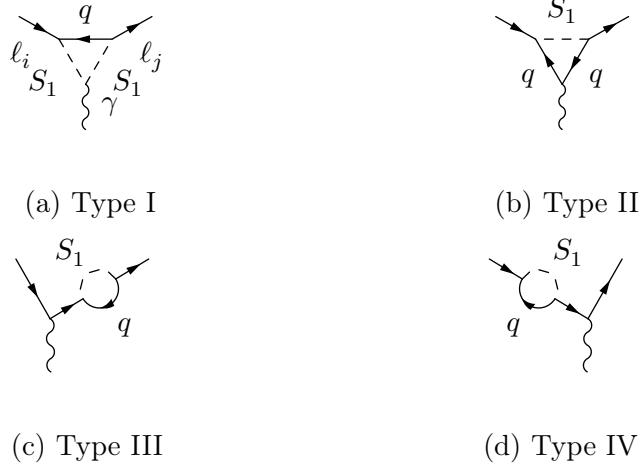


FIG. 2: One-loop diagrams contributing to $\ell_i \rightarrow \ell_j \gamma$ induced by S_1 leptoquark.

δ_{QED} [77, 78], which are also implemented in `FlexibleSUSY`, see Ref. [73]. The loop function themselves are defined as (with following limits for $x \rightarrow 0$: $F_F(x) \approx -9/2 - 3 \ln x$, $F_C(0) = 0$, $F_E(0) = 4$, $F_B(0) = 2$; see also Refs. [37, 79]):

$$\begin{aligned}
 L_1(x) &= 4F_F(x) - F_C(x) > 0, & L_2(x) &= 2F_E(x) - F_B(x) > 0, \\
 F_F(x) &= \frac{3(-3 + 4x - x^2 - 2 \ln x)}{2(1-x)^3}, & F_E(x) &= \frac{2(2 + 3x - 6x^2 + x^3 + 6x \ln x)}{(1-x)^4}, \\
 F_C(x) &= \frac{3(1 - x^2 + 2x \ln x)}{(1-x)^3}, & F_B(x) &= \frac{2(1 - 6x + 3x^2 + 2x^3 - 6x^2 \ln x)}{(1-x)^4}.
 \end{aligned} \tag{7}$$

Note that the first two functions are positive, which allows only constructive interference of contributions from different quark generations (as long as all couplings are positive). The first term in Eq. (6) contains the chirally enhanced ratio m_q/m_μ whereas the second one does not. The chirally enhanced term appears together with a product of two couplings to different fermion chiralities $\lambda_L^{q2} \lambda_R^{q2}$. It is well known that this enhancement is crucial for the possibility to explain a significant leptoquark contribution to Δa_μ .

The theory prediction in Eq. (6) can be compared to the difference between the experimental measurement and the corresponding Standard Model prediction, see Eq. (1).

B. $\ell_i \rightarrow \ell_j \gamma$

The Feynman diagrams contributing to two-body decays $\ell_i \rightarrow \ell_j \gamma$ are similar to the ones contributing to Δa_μ . Figure 2 displays the four contributing types of one-loop diagrams; the main difference is the replacement of the external fermions and associated leptoquark coupling constants.

The contributions of Figure 2 can be expressed as amplitudes with off-shell photon with outgoing momentum $q = p_i - p_j$ (using the conventions of Refs. [80, 81] with the covariant derivative $\mathcal{D}_\mu = \partial_\mu + ieQ_f A_\mu$),

$$i\Gamma_{\bar{\ell}_j \ell_i \gamma} = i\bar{u}_j \left[(q^2 \gamma^\mu - q^\mu \not{q}) \left(A_1^L P_L + A_1^R P_R \right) + im_i \sigma^{\mu\nu} q_\nu \left(A_2^L P_L + A_2^R P_R \right) \right] u_i. \quad (8)$$

The two-body decays of interest only depend on the squares of the dipole form factors $A_2^{L,R}$; the branching ratio has the form (see, e.g. [79, 80]):

$$\text{BR}(\ell_i \rightarrow \ell_j \gamma) = \frac{m_{\ell_i}^5}{16\pi\Gamma_i} \left(|A_2^L|^2 + |A_2^R|^2 \right) \quad (9)$$

with the decay width of muon and tau, $\Gamma_\mu = 2.996 \cdot 10^{-19}$ GeV and $\Gamma_\tau = 2.267 \cdot 10^{-12}$ GeV [82].

The structure of the dipole form factors is analogous to the situation for Δa_μ ,

$$A_2^L = -\frac{1}{16\pi^2} \frac{e}{6m_{S_1}^2} \left(\frac{m_q}{m_i} \lambda_R^{qj} \lambda_L^{qi} L_1(x_q) + \frac{1}{4} \lambda_R^{qj} \lambda_R^{qi} L_2(x_q) \right) < 0. \quad (10)$$

The expressions for A_1 terms will be listed below in the context of three-body decays, where they will be relevant.

The prediction for the two-body decays will be compared to the corresponding experimental upper limits listed in Table I. The existing upper limits on $\mu \rightarrow e\gamma$, $\tau \rightarrow e\gamma$ and $\tau \rightarrow \mu\gamma$ were obtained at MEG [83] BaBar [84], the next foreseeable improvements are planned at MEG-II [85] and Belle-II [86].

C. $\ell_i \rightarrow \ell_j \ell_k \ell_k^c$

Like for Δa_μ and for the two-body decays $\ell_i \rightarrow \ell_j \gamma$, leptoquarks contribute to the three-body decays $\ell_i \rightarrow \ell_j \ell_k \ell_k^c$ starting from the one-loop level. The five types of one-loop diagrams are shown in Figure 3. Type I to IV contain a $\ell_i \rightarrow \ell_j \gamma$ subdiagram but the outgoing on-shell photon is replaced by a virtual photon which finally decays into a lepton-antilepton pair.

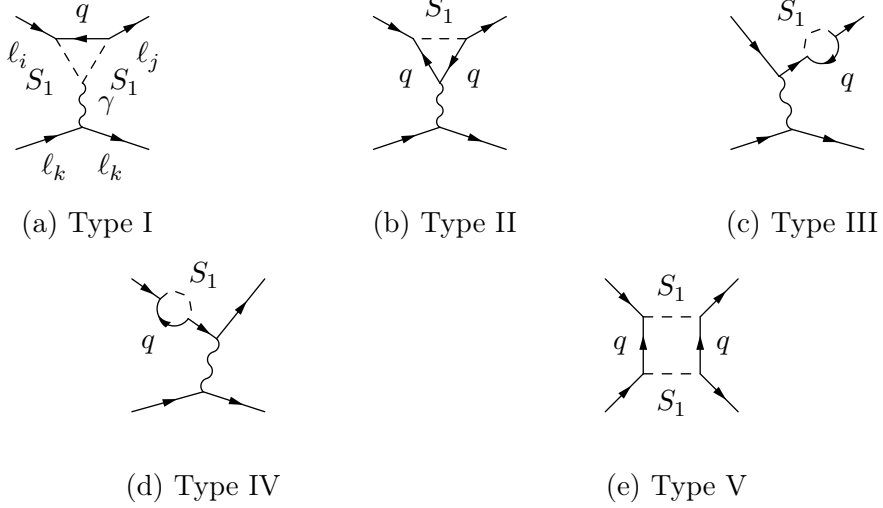


FIG. 3: One-loop diagrams contributing to $\text{BR}(\ell_i \rightarrow \ell_j \ell_k \ell_k^c)$ induced by S_1 leptoquark. Diagrams of type I–IV also have u -channel counterparts. In addition to the box diagram of type V there is an analogous one where leptoquarks propagate as quarks and vice versa. Higgs-boson penguins are negligible for the derivation of the LQ coupling limits due to SM Yukawa magnitude. Z -boson penguins lead to the contribution similar to the A_1 one of the photon but are relatively suppressed due to the mass of the former.

Type V is a box diagram that is distinguished from all other diagrams in that it involves four powers of leptoquark couplings instead of two.

The leptoquark contributions to the three-body decays arise via the dipole form factor and 4-fermion (scalar, vector, and tensor) form factors S_{XY} , V_{XY} , T_{XY} (with X, Y being L or R). The vector form factor receives a contribution not only from actual 4-fermion box diagrams of type V in Figure 3, denoted as V_{XY}^\square , but also from the photonic form factor A_1 defined above in Eq. (8).

The full form of the decay width for $\ell_i \rightarrow \ell_j \ell_k \ell_k^c$ in case of $j = k$ and $j \neq k$ reads, see also Refs. [87–90]:

$$\Gamma_{\ell_i \rightarrow 3\ell_j} = \frac{m_i^5}{192\pi^3} \left(e^2 |A_2^L|^2 \left(\ln \frac{m_i^2}{m_j^2} - \frac{11}{4} \right) + e \left(\frac{3}{2} e A_1^L - \frac{1}{2} (V_{LL}^\square + V_{LR}^\square) \right) |A_2^R| + \frac{1}{4} V_{LL}^2 + \frac{1}{8} V_{LR}^2 + \frac{1}{16} S_{LL}^2 + [L \leftrightarrow R] \right), \quad (11)$$

$$\Gamma_{\ell_i \rightarrow \ell_j \ell_k \ell_k^c} = \frac{m_i^5}{192\pi^3} \left(e^2 |A_2^L|^2 \left(\ln \frac{m_i^2}{m_k^2} - 3 \right) + e \left(e A_1^L - \frac{1}{2} (V_{LL}^\square + V_{LR}^\square) \right) |A_2^R| + \frac{1}{8} (V_{LL}^2 + V_{LR}^2) + \frac{1}{32} (S_{LL}^2 + S_{LR}^2) + \frac{3}{2} T_{LL}^2 + [L \leftrightarrow R] \right). \quad (12)$$

The vectorial photon form factor A_1 and its contribution to the 4-fermion form factors are given by

$$A_1^L = \frac{1}{16\pi^2} \frac{e}{36m_{S_1}^2} L_3(x_q) \lambda_L^{qj} \lambda_L^{qi}, \quad (13)$$

$$V_{XY} = -eA_1^X + nV_{XY}^\square,$$

where the minus sign is related to the form factor embedding into the 4-fermion amplitude, and where a similar equation holds for A_1^R ; $n = \frac{1}{2}$ for V_{XX} in $\ell_i \rightarrow 3\ell_j$, and $n = 1$ otherwise. The loop function takes the form (with the following limit for $x \rightarrow 0$: $F_A(0) = 0$, $F_D(x) \approx 4(4 + 3 \ln x)$):

$$\begin{aligned} L_3(x) &= F_A(x) - 2F_D(x) > 0, \\ F_A(x) &= \frac{2 - 9x + 18x^2 - 11x^3 + 6x^3 \ln x}{(1-x)^4}, \\ F_D(x) &= \frac{16 - 45x + 36x^2 - 7x^3 + 6(2 - 3x) \ln x}{(1-x)^4}. \end{aligned} \quad (14)$$

The pure box diagram contributions can be written as

$$\begin{aligned} S_{LL} &= \frac{1}{16\pi^2} \left(\frac{1}{2} \lambda_L^{q_2 i} \lambda_L^{q_1 k} - \lambda_L^{q_1 i} \lambda_L^{q_2 k} \right) \lambda_R^{q_1 j} \lambda_R^{q_2 k} m_{q_1} m_{q_2} D_0, \\ S_{LR} &= -\frac{1}{16\pi^2} \left(2\lambda_L^{q_2 i} \lambda_R^{q_1 k} |D_{00}| + \lambda_L^{q_1 i} \lambda_R^{q_2 k} m_{q_1} m_{q_2} D_0 \right) \lambda_R^{q_1 j} \lambda_L^{q_2 k}, \\ V_{LL}^\square &= \frac{1}{16\pi^2} \left(\lambda_L^{q_1 i} \lambda_L^{q_2 k} + \lambda_L^{q_2 i} \lambda_L^{q_1 k} \right) \lambda_L^{q_1 j} \lambda_L^{q_2 k} |D_{00}|, \\ V_{LR}^\square &= \frac{1}{16\pi^2} \left(\lambda_L^{q_1 i} \lambda_R^{q_2 k} |D_{00}| + \lambda_L^{q_2 i} \lambda_R^{q_1 k} \frac{1}{2} m_{q_1} m_{q_2} D_0 \right) \lambda_L^{q_1 j} \lambda_R^{q_2 k}, \\ T_{LL} &= \frac{1}{16\pi^2} \lambda_R^{q_1 j} \lambda_R^{q_2 k} \lambda_L^{q_2 i} \lambda_L^{q_1 k} \frac{1}{8} m_{q_1} m_{q_2} D_0 \end{aligned} \quad (15)$$

with expressions for $S_{RL}, S_{RR}, V_{RL}^\square, V_{RR}^\square, T_{RR}$ obtained by replacing $L \leftrightarrow R$; the zero-momenta Passarino-Veltman coefficient functions D_0 and D_{00} [91] can be simplified to for $q = c$ or t :

$$\begin{aligned} m_{S_1}^4 D_0 \Big|_{q_1=q_2} &= \frac{-2 + 2x_q - (1 + x_q) \ln x_q}{(1 - x_q)^3} > 0, \\ m_{S_1}^2 D_{00} \Big|_{q_1=q_2} &= -\frac{1 - x_q^2 + 2x_q \ln x_q}{4(1 - x_q)^3} < 0, \\ m_{S_1}^4 D_0 \Big|_{m_c \rightarrow 0} &= \frac{-1 + x_t - \ln x_t}{(1 - x_t)^2} > 0, \\ m_{S_1}^2 D_{00} \Big|_{m_c \rightarrow 0} &= \frac{-1 + x_t - x_t \ln x_t}{4(1 - x_t)^2} < 0. \end{aligned} \quad (16)$$

The prediction for the three-body decays will be compared to the corresponding experimental upper limits listed in Table I. Most important are the limits on $\mu \rightarrow 3e$. The existing

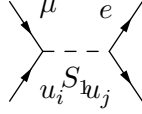


FIG. 4: Tree-level diagram contributing to $\mu Au \rightarrow e Au$ and $\mu Al \rightarrow e Al$.

limits were obtained at SINDRUM [92], and the next foreseen improvement is planned at Mu3e-I [93].

We note that the main contribution from the box factors comes from the D_{00} -terms and that the box form factors in (15) are positive, for positive values of the $\lambda_{L,R}$.

D. $\mu \rightarrow e$ conversion

Out of all considered observables $\mu \rightarrow e$ conversion in presence of a nucleus is special since it is mediated already by a tree-level diagram with leptoquark exchange. Figure 4 shows the diagram. The resulting predicted conversion rate can be expressed as

$$\text{BR}(\mu - e) = \frac{(\alpha_s \lambda_R^{12} - \alpha_v \lambda_L^{12})^2 (\lambda_L^{11})^2 + [L \leftrightarrow R]}{4m_{S_1}^4 \omega_{\text{capt}}} \quad (17)$$

with the capture rate and the form-factors (muon mass and ω_{capt} are expressed in GeV units):

$$\begin{aligned} \alpha_s &= \sum_{i=p,n} f_u^i \frac{m_i}{m_u} S^{(i)} = 1.537 (0.430 \text{ in } Al) \cdot m_\mu^{5/2}, \\ \alpha_v &= 2V^{(p)} + V^{(n)} = 0.280 (0.049 \text{ in } Al) \cdot m_\mu^{5/2}, \\ \omega_{\text{capt}} &= 8.849 (0.464 \text{ in } Al) \cdot 10^{-18}. \end{aligned} \quad (18)$$

The overlap integrals are taken from the second method in Ref. [94]. The proton and neutron scalar couplings $f_u^{p,n}$ are determined from pion-nucleon $\sigma_{\pi N}$ term for u quark (see the Ref. [95] for the numerical values). Vector form-factors 2 and 1 (in α_v) do not suffer from theoretical uncertainty and are derived from the conservation of vector current consideration, i.e. counting of valence quarks.

The past SINDRUM-II and the planned COMET-I (as well as COMET-II and Mu2e [96]) experiments listed in Table I use either Au or Al nuclei for $\mu \rightarrow e$ conversion. The prediction can be applied to both cases, see the first/second numbers in Eq. (18) accordingly.

Observable	Current phase	Next phase
Δa_μ^{2021}	FNAL [2]: $(25.1 \pm 5.9) \cdot 10^{-10}$	—
$\mu \rightarrow e\gamma$	MEG [83]: $4.2 \cdot 10^{-13}$	MEG-II [85]: $6 \cdot 10^{-14}$
$\tau \rightarrow e\gamma$	BaBar [84]: $3.3 \cdot 10^{-8}$	Belle-II [86]: $9.0 \cdot 10^{-9}$
$\tau \rightarrow \mu\gamma$	BaBar [84]: $4.4 \cdot 10^{-8}$	Belle-II [86]: $6.9 \cdot 10^{-9}$
$\mu \rightarrow 3e$	SINDRUM [92]: $1 \cdot 10^{-12}$	Mu3e-I [93]: $2 \cdot 10^{-15}$
$\tau \rightarrow 3e$	Belle-I [99]: $2.7 \cdot 10^{-8}$	Belle-II [86]: $4.7 \cdot 10^{-10}$
$\tau \rightarrow \mu ee$	Belle-I [99]: $1.8 \cdot 10^{-8}$	Belle-II [86]: $2.9 \cdot 10^{-10}$
$\tau \rightarrow e\mu\mu$	Belle-I [99]: $2.7 \cdot 10^{-8}$	Belle-II [86]: $4.5 \cdot 10^{-10}$
$\tau \rightarrow 3\mu$	Belle-I [99]: $2.1 \cdot 10^{-8}$	Belle-II [86]: $3.6 \cdot 10^{-10}$
$\mu Au \rightarrow e Au$	SINDRUM-II [100]: $7 \cdot 10^{-13}$	—
$\mu Al \rightarrow e Al$	—	COMET-I [101]: $7 \cdot 10^{-15}$
$K^+ \rightarrow \pi^+ \nu \bar{\nu}$	E949 [102]: $1.73 \cdot 10^{-10}$	—
$D^0 \rightarrow \mu^+ \mu^-$	LHCb [103]: $7.6 \cdot 10^{-9}$	—

TABLE I: Experimental bounds, that are considered in the present paper. The column “Current phase” refers to current, existing bounds, and the column “Next phase” refers to the next available expected future bound. We use 90 % confidence level (but 1σ -bound in case of Δa_μ). Note, the anomalous magnetic moment of muon and kaon branching ratio are the only quantities corresponding to observations and not upper limits.

IV. ANALYSIS STRATEGY

Our main interest is the impact of Δa_μ and CLFV observables on the full 3×3 coupling matrices $\lambda_{L,R}$, using the experimental bounds listed in Table I. To simplify the analysis, we assume all 18 considered couplings to be positive and apply the customary perturbative upper bound [97, 98]:

$$0 < \lambda_L^{ij} < \sqrt{4\pi}, \quad 0 < \lambda_R^{ij} < \sqrt{4\pi}, \quad (19)$$

on each matrix element.

Possible masses of leptoquarks are constrained by a variety of LHC analyses accumulated

Decay/coupling	β	Lowest allowed mass [GeV]	Reference
ue	1.0 (0.5)	1435 (1270)	$\sqrt{s} = 13$ TeV CMS [104]
ue	1.0 (0.5)	1400 (1290)	$\sqrt{s} = 13$ TeV ATLAS [105]
$\lambda^{ue} = 1.0$ (0.8)	1.0	1755 (1355)	$\sqrt{s} = 8$ TeV CMS [106]
$c\mu$	1.0 (0.5)	1530 (1285)	$\sqrt{s} = 13$ TeV CMS [107]
$c\mu$	1.0 (0.5)	1560 (1230)	$\sqrt{s} = 13$ TeV ATLAS [105]
$\lambda^{c\mu} = 1.0$	1.0	660	$\sqrt{s} = 8$ TeV CMS [106]
$t\mu$	1.0	1420	$\sqrt{s} = 13$ TeV CMS [108]
$t\tau$	1.0	950	$\sqrt{s} = 13$ TeV CMS [109]
$t\tau$	1.0 (0.5)	920 (810)	$\sqrt{s} = 13$ TeV ATLAS [110]
$\lambda^{t\tau} = 2.5$	1.0	1020	$\sqrt{s} = 13$ TeV CMS [109]

TABLE II: LHC constraints on scalar leptoquarks masses at 95% confidence level. The first column shows the decay mode assumed in the analysis, or — for analyses considering single leptoquark production — specifies the assumed value of the relevant coupling. In the second column the quantity β is the leptoquark branching decay ratio into the quark/lepton mentioned in the first column. The numbers without brackets correspond to the strongest achievable bounds, the numbers in brackets correspond to alternative assumptions and corresponding weaker bounds.

in Table II. In this paper, we fix the leptoquark mass in all numerical results below as

$$m_{S_1} = 1.8 \text{ TeV}. \quad (20)$$

This value is conservative as it respects all current LHC restrictions in the third column of Table II.

In our analysis, we focus particularly on three distinct scenarios. This helps manage the 18-dimensional parameter space and draw illuminating and fairly general conclusions. The leptonic observables mainly correlate the coupling matrices $\lambda_{L,R}^{q\ell}$ horizontally — i.e. couplings of the same quark to different leptons. This is different from the case of e.g. B -physics and the constraints from accommodating B -anomalies related to $R(D^{(*)})$ as done e.g. in Ref. [60]. For this reason, our scenarios leave this horizontal direction unconstrained but impose various vertical relationships on the coupling matrices.

Scenario 1, top-only case: Here only couplings to the top-quark are nonzero. We are left with the 6 parameters $\lambda_{L,R}^{3\ell}$, $\ell = 1, 2, 3$.

Scenario 2, charm-only case: Here only couplings to the charm-quark are nonzero. We are left with the 6 parameters $\lambda_{L,R}^{2\ell}$, $\ell = 1, 2, 3$.

Scenario 3, columns case: Here we assume quark-universality of couplings, i.e. assume equal couplings in each column of the coupling matrices, $\lambda_L^{1\ell} = \lambda_L^{2\ell} = \lambda_L^{3\ell} \equiv \lambda_L^\ell$ (and the same for λ_R). We are left with the 6 parameters $\lambda_{L,R}^\ell$, $\ell = 1, 2, 3$.

In addition, we will use the μ - e conversion process to constrain the up-quark couplings $\lambda_{L,R}^{1\ell}$ ($\ell = 1, 2$) in a way independent of assumptions on vertical relationships. In all analyses, we will only consider real couplings. We note that similar but more restrictive scenarios were discussed in Refs. [42, 44, 45, 50–52, 68] to study muon $g - 2$, and similar scenarios allowing for CLFV processes were discussed in Refs. [43, 46–49, 53–55, 69].

V. PHENOMENOLOGICAL CONSEQUENCES OF Δa_μ

We begin our phenomenological investigations with an analysis of Δa_μ . In addition to known results in the literature (see in particular Refs. [37, 50, 68]) we focus on the contributions of all generations and derive bounds on several (combinations of) $\lambda_{L,R}$ -parameters which will be instructive and useful later.

The analytical result was presented in Eq. (6). It contains chirality-flipping terms proportional to $m_q \lambda_L^{q2} \lambda_R^{q2}$ where q is one of the up-type quarks. It is well known that leptoquark models can explain large Δa_μ only via such chirality-flipping terms which are enhanced by the large top- or charm-quark masses.

To provide an overview we first record a criterion under which chirality-flip enhancement is at all possible. In Eq. (6) the relative factors between the chirality-flipping and non-flipping terms are schematically $m_q \lambda_L^{q2} \lambda_R^{q2} L_1 : m_\mu |\lambda_{L,R}^{q2}|^2 L_2$ with loop functions $L_{1,2}$. Inserting typical masses of the order few TeV we obtain restrictions on the ratios between the left- and right-handed couplings corresponding to chiral enhancement:

$$\begin{aligned} \text{charm:} \quad & \frac{1}{700} \lesssim \frac{\lambda_L^{22}}{\lambda_R^{22}} \lesssim 700, \\ \text{top:} \quad & \frac{1}{4 \cdot 10^4} \lesssim \frac{\lambda_L^{32}}{\lambda_R^{32}} \lesssim 4 \cdot 10^4. \end{aligned} \tag{21}$$

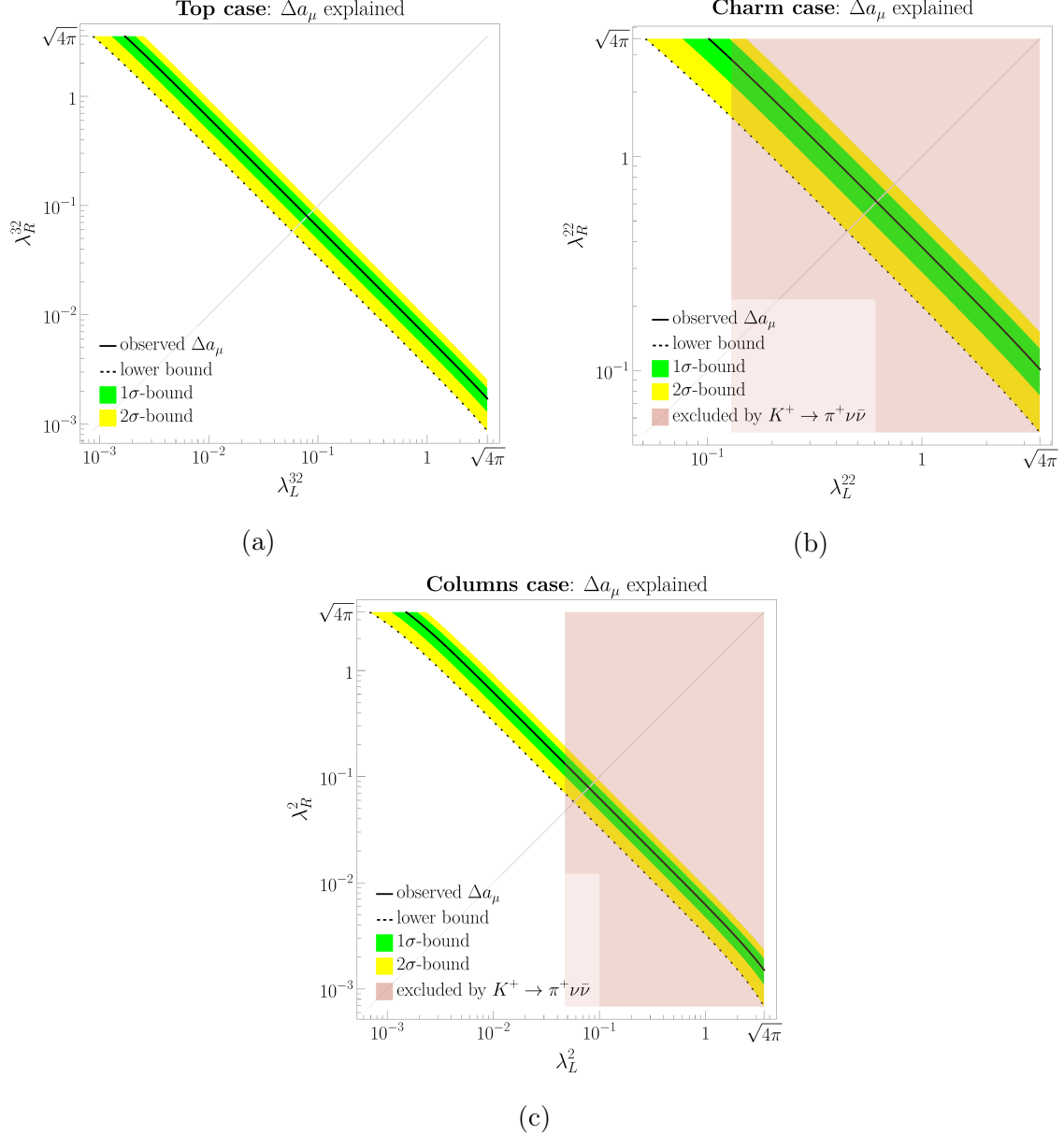


FIG. 5: Bands in parameter space allowed by Δa_μ , for $m_{S_1} = 1.8$ TeV. The three plots correspond to the three different scenarios, defined in Sec. IV. The red-shaded regions correspond to the maximal additional limits from the $K^+ \rightarrow \pi^+ \nu \bar{\nu}$ decay.

In Eq. (21) we have not included the up-quark, since its contributions to Δa_μ are generally small. Indeed, the $K^+ \rightarrow \pi^+ \nu \bar{\nu}$ decay, see Figure 10, implies the restriction $\lambda_L^{12} \lesssim 1$ regardless of all other relevant couplings due to cancellation in \hat{Y}_{12}^L factor, see appendix A 1. With the upper perturbative limit applied for the other coupling $\lambda_R^{12} \lesssim \sqrt{4\pi}$, the maximum contribution of the first quark-generation couplings contributes at most 9% of the Δa_μ mean

value (for $m_{S_1} = 1.8$ TeV). This number falls drastically for heavier leptoquark mass and/or smaller couplings. Hence, one can to a very good extent neglect the up-quark contributions and focus on the ones from heavier quarks.

Now we focus on the first of our scenarios and consider the *top-couplings* $\lambda_{L,R}^{32}$ and their values required to explain Δa_μ , while the charm-/up-quark couplings are set to zero.

Due to $m_t/m_\mu \sim O(10^3)$ the full prediction for Δa_μ of Eq. (6) can be well approximated (if the coupling ratio is in the range (21)) by the chirality-flipping term, which in turn can be approximated as (*top-only scenario*)

$$\Delta a_\mu \approx 3.3 \cdot 10^{-7} \frac{1 + 0.64 \ln(m_{S_1}/2 \text{ TeV})}{(m_{S_1}/2 \text{ TeV})^2} \lambda_L^{32} \lambda_R^{32}, \quad (22)$$

which highlights the dependence on the couplings and allows to read off easily the values for masses in the few-TeV range.

From comparing with the experimental result we get bounds on products of the two couplings that are approximately located within hyperbolic curves in the $\lambda_L^{32} - \lambda_R^{32}$ plane. This is shown in the double logarithmic scale in Figure 5a, where the hyperbolic shape becomes a straight band. The plot shows the coupling values for which the experimental Δa_μ result is explained at the 1σ (2σ) level in green (yellow). The plot is obtained from the exact Eq. (6), hence there is an $\mathcal{O}(10\%)$ distortion from the hyperbolic shape due to the non-chirally enhanced terms.

Despite the small distortion, the band in Figure 5a essentially restricts the product of the left- and right-handed top-couplings to the muon. As a simple formula, the entire 2σ band is confined in the interval (*top-only scenario*)

$$\Delta a_\mu \text{ band: } 3.1 \cdot 10^{-3} < \lambda_L^{32} \lambda_R^{32} < 9.3 \cdot 10^{-3}. \quad (23)$$

If we apply the perturbativity upper limit $\sqrt{4\pi}$ on each individual coupling, the product (23) implies also lower limits on each coupling (*top-only scenario*):

$$2\sigma \text{ individual limit: } 8.7 \cdot 10^{-4} < \lambda_{L,R}^{32}. \quad (24)$$

Note that the 2σ label here does not have a direct statistical meaning but refers to the 2σ bound of Figure 5a from which the limit is derived.

As a by-product, this equation also implies a possible range of the ratio of couplings $\lambda_L^{32} : \lambda_R^{32}$ between around $1/4000 \dots 4000$, which is a sharpened version of Eq. (21) derived only from chirality-flip dominance.

Now we repeat the analysis for the second scenario and consider explaining Δa_μ purely with the *charm-couplings* $\lambda_{L,R}^{22}$, setting the top-/up-quark couplings to zero. The ratio $m_c/m_\mu \sim O(10)$ is smaller than the one for the top-quark. Nevertheless, it makes the chirally enhanced term still dominate such that the non-chirally enhanced term can be neglected to estimate how strongly the relevant couplings are restricted.

Applying similar simplifications as in the top case one obtains the following approximation which highlights the dependence on the couplings and is valid in the few-TeV range (*charm-only scenario*):

$$\Delta a_\mu \approx 5.4 \times 10^{-9} \frac{1 + 0.14 \ln(m_{S_1}/2 \text{ TeV})}{(m_{S_1}/2 \text{ TeV})^2} \lambda_L^{22} \lambda_R^{22}. \quad (25)$$

Figure 5b shows the corresponding bands in the $\lambda_L^{22} - \lambda_R^{22}$ plane explaining the measured Δa_μ at the 1σ and 2σ level. The distortion of the hyperbolic shape is stronger compared to the top-quark case because the dominance of the chirality-flipping contributions is less pronounced. Still, it is essentially the product of the two couplings which matters for Δa_μ , and it is again meaningful to provide the interval of the coupling product for the entire 2σ band (*charm-only scenario*):

$$\Delta a_\mu \text{ band: } 0.18 < \lambda_L^{22} \lambda_R^{22} < 0.56. \quad (26)$$

As shown in Ref. [50], there is a bound from the measurement of $\text{BR}(K^+ \rightarrow \pi^+ \nu \bar{\nu})$ which imposes an additional restriction on the coupling λ_L^{22} .² However, the bound significantly depends on λ_L^{12} : for lower values we obtain the result from [50], for larger ones λ_L^{22} becomes unrestricted. This behavior is illustrated by the upper boundary of the green area in the Figure 10 of the appendix A 1. If one sets the coupling λ_L^{12} to zero, which implies the maximally restrictive bound from the $K^+ \rightarrow \pi^+ \nu \bar{\nu}$ decay, then the excluded region is shown in Figure 5b as the pink area.

Similarly to the top-case, applying the perturbativity upper limit on each coupling together with Eq. (26) leads to lower limits on each coupling. These lower limits, and the additional limits from the $K^+ \rightarrow \pi^+ \nu \bar{\nu}$ decay (which applies for the specific case where λ_L^{12}

² In addition, Drell-Yan dilepton processes $pp \rightarrow \mu^+ \mu^-$ and $pp \rightarrow \mu^+ \mu^- j$ provide an upper allowed value for λ_R^{22} as function of λ_L^{22} and m_{S_1} , see Ref. [50, 111–113]. This upper bound excludes part of the 2σ bound for the charm-only scenario in Eq. (26). We do not use this upper bound here, because for us, it is the lower bound on the couplings in Eq. (26), which impacts the analyses in the remainder of the paper.

vanishes) can be summarized as (*charm-only scenario*)

$$\begin{aligned}
2\sigma \text{ individual limit: } & 5.1 \cdot 10^{-2} < \lambda_{L,R}^{22}, \\
K^+ \rightarrow \pi^+ \nu \bar{\nu} \text{ limits: } & \lambda_L^{22} < 0.13, \quad 1.5 < \lambda_R^{22}.
\end{aligned}
\tag{27}$$

Finally, we focus on the third scenario, the *columns case* where the leptoquark couplings are universal over the quark generations. In this case, Δa_μ is dominated by top-quark contributions and the bounds on the universal couplings are similar to the ones in the top-only case, however the additional limits from the $K^+ \rightarrow \pi^+ \nu \bar{\nu}$ decay are driven by a combination of up- and charm-quark couplings. The corresponding plot is shown in Figure 5c, and the limits are (*columns scenario*)

$$\begin{aligned}
\Delta a_\mu \text{ band: } & 2.4 \cdot 10^{-3} < \lambda_L^2 \lambda_R^2 < 9.2 \cdot 10^{-3}, \\
2\sigma \text{ individual limit: } & 6.8 \cdot 10^{-4} < \lambda_{L,R}^2, \\
K^+ \rightarrow \pi^+ \nu \bar{\nu} \text{ limits: } & \lambda_L^2 < 4.7 \cdot 10^{-2}, \quad 7.0 \cdot 10^{-2} < \lambda_R^2.
\end{aligned}
\tag{28}$$

VI. PHENOMENOLOGICAL CONSEQUENCES OF TWO-BODY DECAYS $\mu \rightarrow e\gamma$, $\tau \rightarrow e\gamma$, AND $\tau \rightarrow \mu\gamma$

A. Consequences of decays involving muons

Now we consider the impact of CLFV on the leptoquark couplings, with special focus on the condition that the current Δa_μ is explained. The first set of CLFV observables are the decays $\mu \rightarrow e\gamma$ and $\tau \rightarrow \mu\gamma$. These have the common feature that, like Δa_μ , they involve the muon and are governed by a dipole interaction which can be dominated by chirality-flipping terms.

We begin with the analysis of the top-related couplings λ_L^{3i} and λ_R^{3i} in scenario 1 (see Sec. IV), where the up- and charm-related couplings are assumed to vanish. Like for Δa_μ , see Eq. (22), an instructive approximation is obtained by taking only the chirally enhanced terms in the formula (9) for the decays $\ell_i \rightarrow \ell_j \gamma$. In this approximation, the limits on branching ratios from Table I translate into the following inequality (all masses are to be given in units of GeV; *top-only scenario*):

$$|\lambda_R^{3i} \lambda_L^{3j}|^2 + |\lambda_L^{3i} \lambda_R^{3j}|^2 < \frac{\Gamma_i \text{BR}(\ell_i \rightarrow \ell_j \gamma)}{m_i^3} \frac{0.73 m_{S_1}^4}{(1 - 0.17 \ln m_{S_1})^2}.
\tag{29}$$

For fixed i, j , this is a limit on a combination of four couplings. There are several ways to extract more detailed information on bounds.

First we may fix the couplings $\lambda_{L,R}^{32}$ relevant for Δa_μ such that the experimental Δa_μ is explained, i.e. fix a point in the band of Figure 5a. In this way, two out of the four couplings are fixed, and e.g. for $\mu \rightarrow e\gamma$, Eq. (29) takes the structure $a|\lambda_L^{31}|^2 + b|\lambda_R^{31}|^2 < c$, i.e. it restricts the remaining two couplings onto an ellipse.

It turns out that the unification of all such ellipses is essentially a hyperbolic region. This observation allows to decouple the influence of the Δa_μ -related couplings from consideration. Figure 6a shows the corresponding allowed parameter regions in the plane of the two couplings λ_L^{31} and λ_R^{31} . It is obtained from a scan over parameters (for $m_{S_1} = 1.8$ TeV), requiring that λ_L^{32} and λ_R^{32} are chosen such that the Δa_μ prediction is within a 2σ band around the measured value quoted in Table I. The yellow (blue) regions are allowed by the bounds of the ‘‘current phase’’ (‘‘next phase’’) experiments in Table I. Figure 7a is analogous but for the decay $\tau \rightarrow \mu\gamma$ and for the couplings λ_L^{33} and λ_R^{33} .

To explain the shape of the allowed regions, we at first introduce auxiliary variables that are the ratio of left and right couplings:

$$k_{ij} = \frac{\lambda_L^{ij}}{\lambda_R^{ij}}, \quad (30)$$

and rewrite the limit in Eq. (29) for $m_{S_1} = 1.8$ TeV equivalently as (*top-only scenario*)

$$\begin{aligned} \lambda_L^{31} \lambda_R^{31} \lambda_L^{32} \lambda_R^{32} &< 3.0 \cdot 10^{-2} \text{ BR}(\mu \rightarrow e\gamma) \frac{k_{31} k_{32}}{k_{31}^2 + k_{32}^2}, \\ \lambda_L^{33} \lambda_R^{33} \lambda_L^{32} \lambda_R^{32} &< 4.8 \cdot 10^{-2} \text{ BR}(\tau \rightarrow \mu\gamma) \frac{k_{33} k_{32}}{k_{33}^2 + k_{32}^2}. \end{aligned} \quad (31)$$

The k_{ij} -dependent factor is maximal for equal k_{ij} ratios and together with the minimal Δa_μ -allowed product of 32-couplings, see Eq. (23), provides the most conservative (in the case of purely top-related couplings) bounds on the product of couplings. These bounds take the announced hyperbolic shape, i.e. they depend only on the products of two couplings (*top-only scenario*):

$$\begin{aligned} \mu \rightarrow e\gamma \Big|_{\Delta a_\mu} &: \lambda_L^{31} \lambda_R^{31} < 2.1 \cdot 10^{-12} \rightarrow 2.9 \cdot 10^{-13}, \\ \tau \rightarrow \mu\gamma \Big|_{\Delta a_\mu} &: \lambda_L^{33} \lambda_R^{33} < 3.5 \cdot 10^{-4} \rightarrow 5.4 \cdot 10^{-5}. \end{aligned} \quad (32)$$

Here and in the following the first (second) number on the right-hand sides correspond to the ‘‘current phase’’ (‘‘next phase’’) experiments and the yellow (blue) regions in Figures 6a

and 7a. In the figures (with logarithmic scale) these hyperbolic limits are visible as the inclined lines.

Figures 6a and 7a also show that the hyperbolic shape is cut off by individual upper limits on each coupling (*top-only scenario*):

$$\begin{aligned} \mu \rightarrow e\gamma|_{\Delta a_\mu} : \lambda_{L,R}^{31} < 1.3 \cdot 10^{-4} \rightarrow 4.9 \cdot 10^{-5}, \\ \tau \rightarrow \mu\gamma|_{\Delta a_\mu} : \lambda_{L,R}^{33} < 1.7 \quad \rightarrow 0.66. \end{aligned} \tag{33}$$

They can be understood in two ways. On the one hand, the perturbativity upper limit together with Δa_μ implies individual lower limits on the Δa_μ -related couplings. Via Eq. (29) this translates into the individual upper limits (33). On the other hand, Eq. (24) implies that k_{32} is bounded. Hence for very large/very small k_{31} the k -dependent factor in Eq. (31) decreases, again explaining the upper bounds on individual couplings in Figures 6a and 7a.

We repeat the previous discussion for the second scenario where only charm-quark couplings are non-zero. The analysis and conclusions proceeds analogously to the previous case where top-quark couplings were non-vanishing.

The four relevant charm-quark couplings for the decay $\ell_i \rightarrow \ell_j \gamma$ are $\lambda_{L,R}^{2i}$ and $\lambda_{L,R}^{2j}$. The semi-numerical approximation for the general bound on the combination of these four couplings reads (all quantities with unit of mass are to be given in units of GeV; *charm-only scenario*):

$$|\lambda_R^{2i} \lambda_L^{2j}|^2 + |\lambda_L^{2i} \lambda_R^{2j}|^2 < \frac{\Gamma_i \text{BR}(\ell_i \rightarrow \ell_j \gamma)}{m_i^3} \frac{1.2 \cdot 10^7 m_{S_1}^4}{(1 - 2.4 \ln m_{S_1})^2}. \tag{34}$$

This limit in Eq. (34) can be rewritten by using the ratios k_{ij} between left- and right-handed couplings, see Eq. (30). For the mass $m_{S_1} = 1.8$ TeV we obtain (*charm-only scenario*)

$$\begin{aligned} \lambda_L^{21} \lambda_R^{21} \lambda_L^{22} \lambda_R^{22} < 1.1 \cdot 10^2 \text{BR}(\mu \rightarrow e\gamma) \frac{k_{21} k_{22}}{k_{21}^2 + k_{22}^2}, \\ \lambda_L^{23} \lambda_R^{23} \lambda_L^{22} \lambda_R^{22} < 1.7 \cdot 10^5 \text{BR}(\tau \rightarrow \mu\gamma) \frac{k_{23} k_{22}}{k_{23}^2 + k_{22}^2}. \end{aligned} \tag{35}$$

Combining these upper limits with lower limits on couplings derived from assuming an explanation of Δa_μ in Eq. (26) yields upper limits on products of only two couplings relevant for each decay (*charm-only scenario*):

$$\begin{aligned} \mu \rightarrow e\gamma|_{\Delta a_\mu} : \lambda_L^{21} \lambda_R^{21} < 1.2 \cdot 10^{-10} \rightarrow 1.8 \cdot 10^{-11}, \\ \tau \rightarrow \mu\gamma|_{\Delta a_\mu} : \lambda_L^{23} \lambda_R^{23} < 2.1 \cdot 10^{-2} \rightarrow 3.2 \cdot 10^{-3}. \end{aligned} \tag{36}$$

The corresponding bounds are visualized in the plots of Figures 6b and 7b. As in the case of the top-quark couplings, the allowed regions correspond to essentially hyperbolic shapes as can be understood from Eq. (36).

Like in the top-coupling case, the figures also show that there are cutoffs for individual couplings. They arise from the lower limits on Δa_μ -related couplings of Eq. (27). There are general cutoffs related to the perturbativity limit combined with requiring a Δa_μ explanation. And there are even stronger cutoffs on the left-handed couplings related to the $K^+ \rightarrow \pi^+ \nu \bar{\nu}$ decay which, via Δa_μ , implies a lower limit on λ_R^{22} . Numerically, the upper limits on individual couplings related to the $\mu \rightarrow e\gamma$ and $\tau \rightarrow \mu\gamma$ decays read (*charm-only scenario*, individual limits):

$$\begin{aligned}
\mu \rightarrow e\gamma|_{\Delta a_\mu} : \lambda_{L,R}^{21} &< 1.3 \cdot 10^{-4} \rightarrow 5.0 \cdot 10^{-5}, \\
\lambda_L^{21} &< 4.6 \cdot 10^{-6} \rightarrow 1.7 \cdot 10^{-6}, \\
\tau \rightarrow \mu\gamma|_{\Delta a_\mu} : \lambda_{L,R}^{23} &< 1.7 \rightarrow 0.67, \\
\lambda_L^{23} &< 6.0 \cdot 10^{-2} \rightarrow 2.3 \cdot 10^{-2},
\end{aligned} \tag{37}$$

where the second/fourth lines correspond to the constraints from the $K^+ \rightarrow \pi^+ \nu \bar{\nu}$ decay.

Turning to the third scenario with quark-universal couplings, the analysis proceeds similar to the previous cases. We just provide the results, which can also be read off from Figures 6c and 7c. The limits on the coupling products are similar to the top-only case since the top-quark provides the dominant contribution (*columns scenario*):

$$\begin{aligned}
\mu \rightarrow e\gamma|_{\Delta a_\mu} : \lambda_L^1 \lambda_R^1 &< 2.5 \cdot 10^{-12} \rightarrow 3.6 \cdot 10^{-13}, \\
\tau \rightarrow \mu\gamma|_{\Delta a_\mu} : \lambda_L^3 \lambda_R^3 &< 4.3 \cdot 10^{-4} \rightarrow 6.7 \cdot 10^{-5}.
\end{aligned} \tag{38}$$

Similarly, the individual limits from Δa_μ together with perturbativity are similar to the case of the top-quark, however the additional limits from $K^+ \rightarrow \pi^+ \nu \bar{\nu}$ decay are different due to the combined contributions from up- and charm-quarks (*columns scenario*, individual limits):³

³ The limits on couplings obtained in this section supersede the ones coming from Δa_e [64, 114] and Δa_τ [115, 116] under the assumption of Δa_μ , thus the former are not mentioned in this paper.

$$\begin{aligned}
\mu \rightarrow e\gamma|_{\Delta a_\mu} : \lambda_{L,R}^1 &< 1.6 \cdot 10^{-4} \rightarrow 6.1 \cdot 10^{-5}, \\
\lambda_L^1 &< 1.8 \cdot 10^{-6} \rightarrow 7.0 \cdot 10^{-7}, \\
\tau \rightarrow \mu\gamma|_{\Delta a_\mu} : \lambda_{L,R}^3 &< 2.1 \rightarrow 0.83, \\
\lambda_L^3 &< 2.4 \cdot 10^{-2} \rightarrow 9.5 \cdot 10^{-3}.
\end{aligned} \tag{39}$$

B. Consequences for $\tau \rightarrow e\gamma$

Here we consider the decay $\tau \rightarrow e\gamma$. It is also dipole-induced and chirality-flip enhanced, but it is not connected to Δa_μ -related couplings. The decay can be analyzed analogously to $\mu \rightarrow e\gamma$ and $\tau \rightarrow \mu\gamma$, and we present only results for the two generation-specific scenarios. For the top-only case this leads to the constraint (*top-only scenario*)

$$\tau \rightarrow e\gamma : \lambda_L^{31} \lambda_R^{31} \lambda_L^{33} \lambda_R^{33} < 8.0 \cdot 10^{-7} \rightarrow 2.2 \cdot 10^{-7}. \tag{40}$$

Here, a k -dependent factor similar to the ones in Eq. (31) has been maximized to obtain the most conservative bound. We see that the bound involves the same four couplings as the ones of Eq. (32) restricted by $\mu \rightarrow e\gamma$ and $\tau \rightarrow \mu\gamma$, but it is considerably weaker: if the limits in Eq. (32) are met, the additional bound of Eq. (40) is automatically satisfied by many orders of magnitude.

The analogous result for the case of purely charm-quark couplings reads (*charm-only scenario*)

$$\tau \rightarrow e\gamma : \lambda_L^{21} \lambda_R^{21} \lambda_L^{23} \lambda_R^{23} < 2.8 \cdot 10^{-3} \rightarrow 7.7 \cdot 10^{-4}. \tag{41}$$

Again, this limit is many orders of magnitude weaker than the combination of limits derived from $\mu \rightarrow e\gamma$ and $\tau \rightarrow \mu\gamma$ under the assumption of an explanation of Δa_μ in Eq. (36).

VII. PHENOMENOLOGICAL CONSEQUENCES OF THREE-BODY DECAYS $\mu \rightarrow 3e$ AND OTHERS

The phenomenological discussion of three-body decays $\ell_i \rightarrow \ell_j \ell_k \ell_k^c$, particularly of $\mu \rightarrow 3e$, can be kept brief. Even though these processes are influenced by a variety of vertex and box form factors, they are strongly dominated by the dipole form factors $A_2^{L,R}$ in those parts of parameter space which gives rise to conservative bounds aimed for in the present study. For

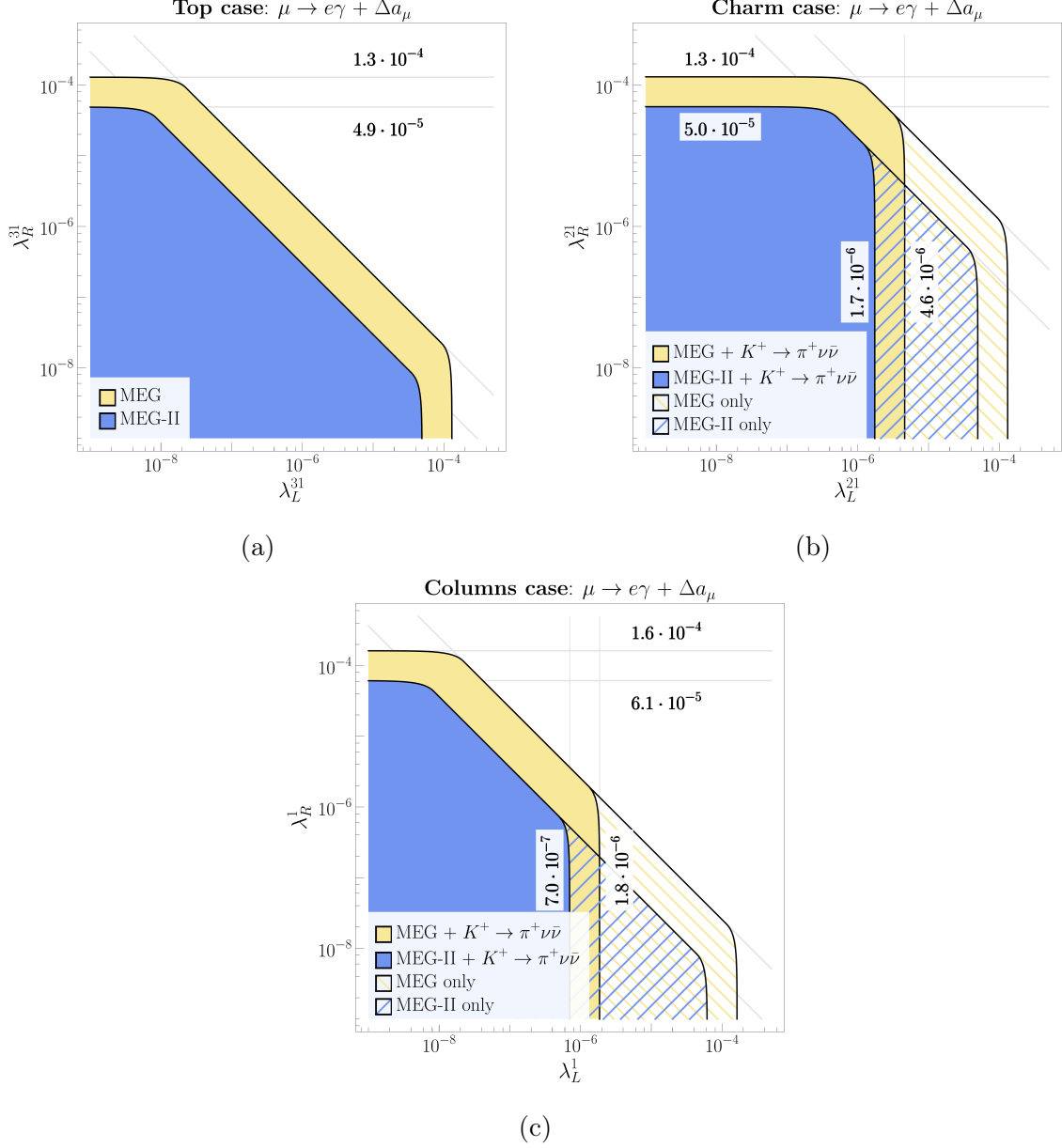


FIG. 6: Allowed parameter regions for the $\mu \rightarrow e\gamma$ decay, assuming that Δa_μ is explained, with $m_{S_1} = 1.8$ TeV, and for the three different scenarios defined in Sec. IV. The meaning of the additional limits from the $K^+ \rightarrow \pi^+ \nu \bar{\nu}$ decay is as in Figure 5.

this purpose the three-body decays are strongly correlated to the simpler two-body decays $\ell_i \rightarrow \ell_j \gamma$.

The dipole dominance is illustrated in Figure 8, which shows the ratio of the two predicted branching ratios for the two most interesting processes $\mu \rightarrow 3e$ and $\mu \rightarrow e\gamma$, for a range of $\lambda_{L,R}$. The color code of the points corresponds to the spread between the four relevant

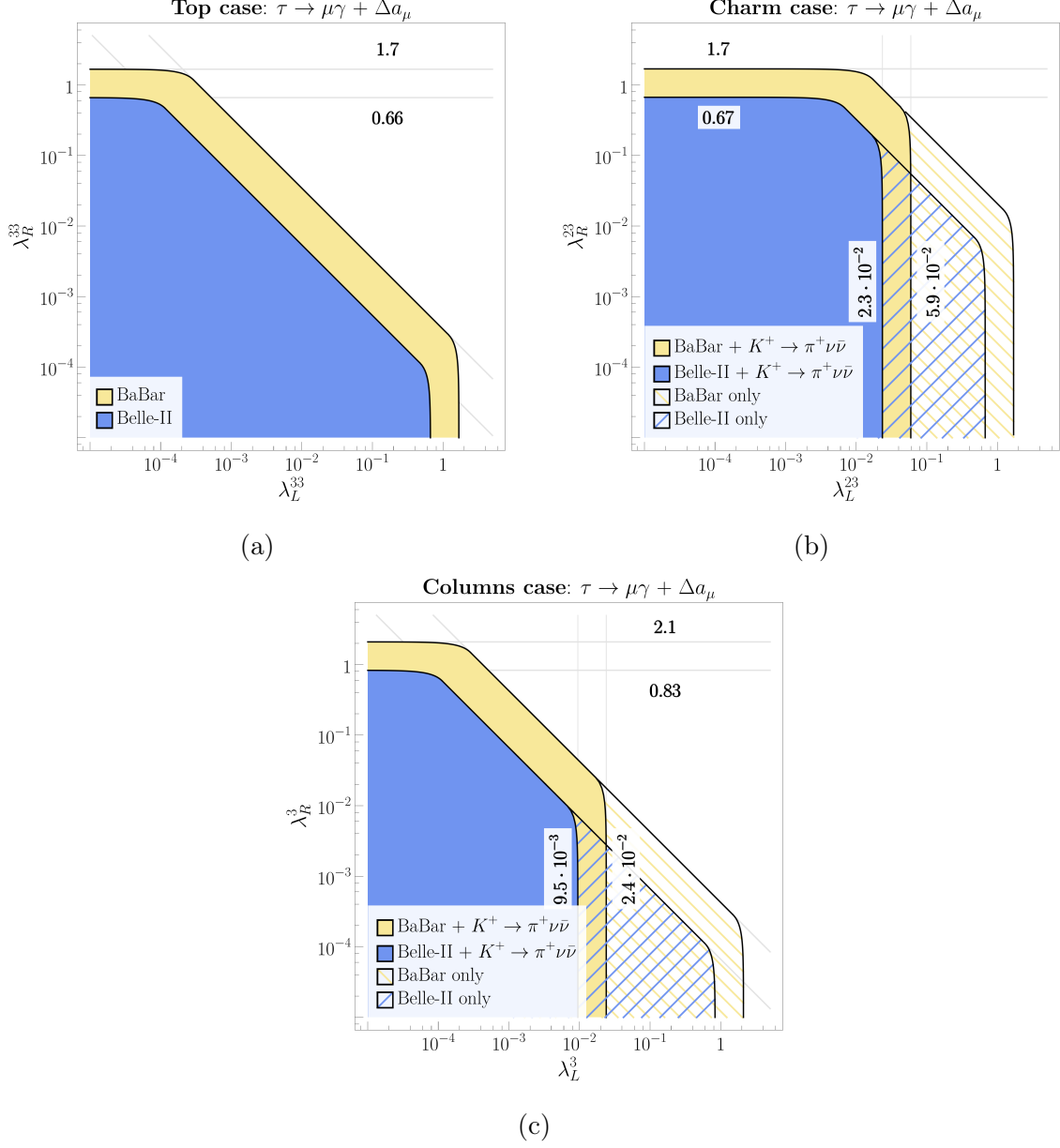


FIG. 7: As Figure 6 but for the $\tau \rightarrow \mu\gamma$ decay.

couplings $\lambda_{L,R}^{31}$ and $\lambda_{L,R}^{32}$ in case of scenario 1. If the spread is moderate (green/blue points), we have an essentially fixed ratio between the branching ratios for $\mu \rightarrow 3e$ and $\mu \rightarrow e\gamma$, which is approximately

$$\frac{\text{BR}(\mu \rightarrow 3e)}{\text{BR}(\mu \rightarrow e\gamma)} = 6.6 \cdot 10^{-3}. \quad (42)$$

The dipole dominance in this parameter region has two reasons.

First, the photonic form factor $A_1^{L,R}$ behaves similarly to the non-chirally enhanced terms in the dipole form factor $A_2^{L,R}$. Since we are working in a coupling regime with strong

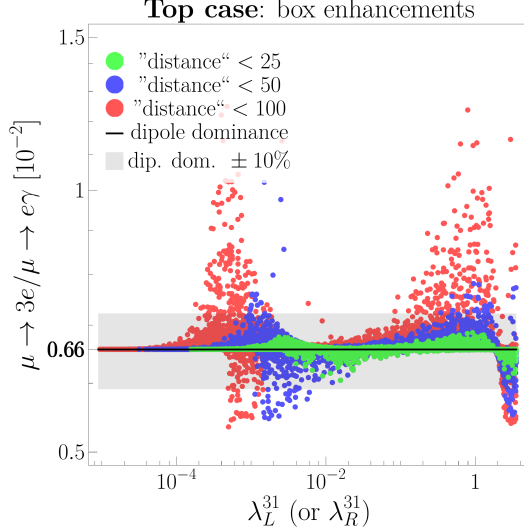


FIG. 8: Predicted ratios of the branching ratios for $\mu \rightarrow 3e$ and $\mu \rightarrow e\gamma$, for a range of $\lambda_{L,R}^{31}$, resulting from a scan over the relevant couplings, for $m_{S_1} = 1.8$ TeV. The gray band shows the value of equation (42) for dipole dominance (with a $\pm 10\%$ corridor), and the color code of points corresponds to the spread between the four relevant couplings $\lambda_{L,R}^{31}$ and $\lambda_{L,R}^{32}$ in case of scenario 1. This “distance” is computed by taking the four relevant couplings, calculating their geometric mean, and then determining the maximum difference to the mean, divided by the mean.

chirality-flip enhancements, see Eq. (21), $A_1^{L,R}$ provides only a negligible correction.

Second, the box diagrams (giving rise to contributions to vector, scalar and tensor form factors) are in principle of general interest since they depend on four powers of $\lambda_{L,R}$. However, if the spread between the couplings is moderate this cannot lead to enhancements, resulting in the correlation (42).

However, if a large spread is allowed (red points in Figure 8), the behavior is more complicated and either enhancement or destructive interference is possible.

On the one hand, the derivation of conservative bounds in the style of the figures of Sec. VI depends on the parameter points without box enhancements. Hence, given the available experimental limits of Table I, the three-body decays do not provide additional constraints on top of the ones obtained from two-body decays analyzed in the previous section. This remains true even for the next phases of the experiments listed in Table I.

On the other hand, the enhanced red points show that future $\mu \rightarrow 3e$ measurements are promising since enhanced rates are possible in this leptoquark model. Finally, the planned

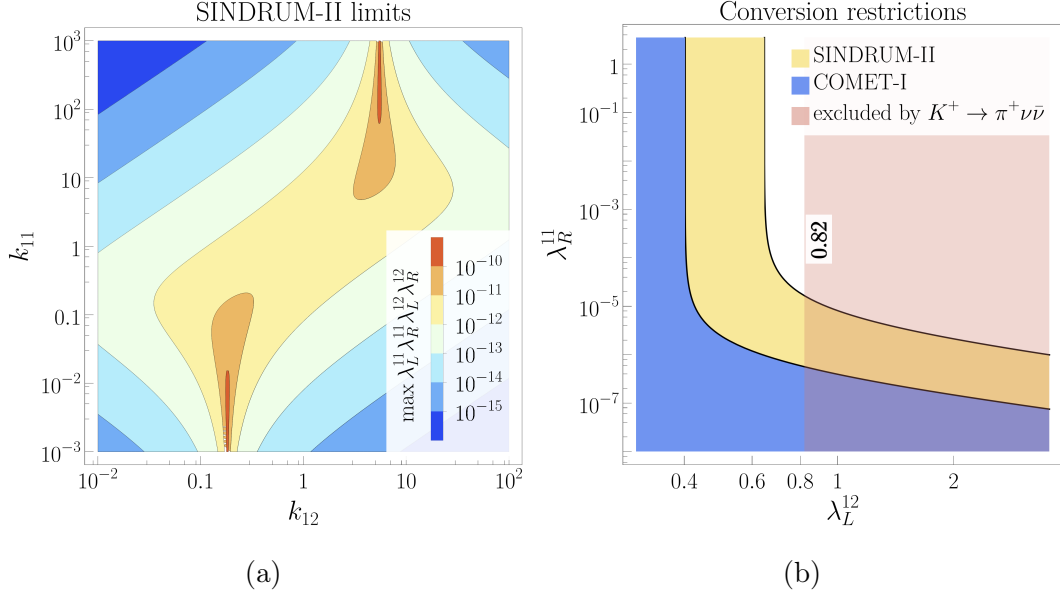


FIG. 9: Limits for $\mu Au \rightarrow e Au$ (SINDRUM-II) and $\mu Al \rightarrow e Al$ (COMET-I) for $m_{S_1} = 1.8$ TeV and different coupling patterns. For Figure 9a see equation (45), and for Figure (9b) see Eq. 48. The red shaded area is fully excluded by the $K^+ \rightarrow \pi^+ \nu \bar{\nu}$ decay.

Mu3e-II [93] experiment for $\mu \rightarrow 3e$, which we otherwise do not consider in the present paper has significant potential for discovery and for improvements of bounds even on the dipole form factors beyond the limits presented in Sec. VI.

VIII. PHENOMENOLOGICAL CONSEQUENCES OF $\mu \rightarrow e$ CONVERSION

To discuss the phenomenological impact of $\mu - e$ conversion process we rewrite the leptoquark contribution in a way similar to the previous observables, as a product of the four relevant couplings and a k_{ij} -dependent factor, as

$$\text{BR}(\mu - e) = \frac{\alpha_s^2}{4m_{S_1}^4 \omega_{\text{capt}}} \lambda_L^{11} \lambda_R^{11} \lambda_L^{12} \lambda_R^{12} k_\alpha. \quad (43)$$

This highlights that the four relevant couplings are $\lambda_{L,R}^{11}$ and $\lambda_{L,R}^{12}$. The dimensionless k_{ij} -dependent factor is denoted as k_α ; it is more involved than for previous cases and this time also depends on the form factors $\alpha_{s,v}$,

$$k_\alpha = \frac{\left(k_{12} - \frac{\alpha_v}{\alpha_s}\right)^2}{k_{11} k_{12}} + k_{11} k_{12} \left(\frac{1}{k_{12}} - \frac{\alpha_v}{\alpha_s}\right)^2. \quad (44)$$

Similarly to the previous observables we can obtain a limit on the product of the four relevant couplings, now depending on the factor k_α . Given the present experimental bound from the SINDRUM-II experiment (or the expected bounds from COMET-I), this limit reads. Note, that form factors $\alpha_{s,v}$ in k_α should be taken appropriately to the nucleus from Eq. (18).

$$\lambda_L^{11} \lambda_R^{11} \lambda_L^{12} \lambda_R^{12} < \frac{8.4 \cdot 10^{-12}}{k_\alpha^{Au}} \rightarrow \frac{5.6 \cdot 10^{-14}}{k_\alpha^{Al}}. \quad (45)$$

Figure 9a displays this limit for the case of the present bound from the SINDRUM-II experiment. In the figure, the color code corresponds to the upper limit on the coupling product, on the axes the two ratio variables k_{11} and k_{12} are varied. The shape of the figure can be explained as follows.

Within the k -dependent factor there can be cancellations: if either $k_{12} = \alpha_v/\alpha_s$ or $k_{12} = \alpha_s/\alpha_v$, the prefactor of the first (or second) term in Eq. (44) vanishes. If simultaneously k_{11} becomes very small (or large), the entire factor k_α is very small, and conversely very large coupling products are allowed. This explains the two horizontal strips in the figure where the limit becomes significantly weaker.

Given this complicated behavior, it is instructive to record the limit in some special cases with different degree of possible cancellations. First, in the special point where $k_{11} = k_{12} = 1$, i.e. where the left- and right-handed couplings happen to be equal, the limits become

$$\begin{aligned} \mu Au \rightarrow eAu|_{\lambda_L=\lambda_R} : \quad & \lambda_{L,R}^{11} \lambda_{L,R}^{12} < 2.5 \cdot 10^{-6}, \\ \mu Al \rightarrow eAl|_{\lambda_L=\lambda_R} : \quad & \lambda_{L,R}^{11} \lambda_{L,R}^{12} < 1.9 \cdot 10^{-7}. \end{aligned} \quad (46)$$

Second, we consider the region where the left- and right-handed couplings may differ by up to a factor 10, $k_{11}, k_{12} \in [0.1, 10]$. In this region one of the terms within k_α can vanish, and overall k_α turns out to vary in the interval $k_\alpha = 0.48 \dots 96$ ($0.73 \dots 98$ for COMET-I). A limit on the coupling product which is valid in all of the region for $m_{S_1} = 1.8$ TeV reads:

$$\lambda_L^{11} \lambda_R^{11} \lambda_L^{12} \lambda_R^{12} < 6.5 \cdot 10^{-12} \rightarrow 3.7 \cdot 10^{-14}. \quad (47)$$

The previous observables have allowed (in conjunction with Δa_μ) to obtain bounds on individual couplings which are complementary to the bounds on coupling products. This is more difficult in the case of $\mu Al \rightarrow eAl$ or $\mu Au \rightarrow eAu$. A major reason is the possibility of cancellations due to the two terms involving α_s and α_v . It is, however, possible to obtain

rather strict limits on the correlation of a subset of two couplings. This is illustrated in Figure 9b, which shows the allowed regions in the plane of the two couplings $\lambda_L^{12}-\lambda_R^{11}$. The remaining two parameters have been scanned over. (A similar plot could be shown in the $\lambda_R^{12}-\lambda_L^{11}$ plane.)

To explain the shape of the plot it is useful to discuss Eq. (17) (or Eq. (44)) distinguishing two cases for the couplings: either we have $\lambda_L^{12} > \frac{\alpha_v}{\alpha_s}\sqrt{4\pi}$ or we have $\lambda_L^{12} \leq \frac{\alpha_v}{\alpha_s}\sqrt{4\pi}$. In the first case, no matter what the value of λ_R^{11} is, the prefactor of λ_R^{11} in the branching ratio is not zero; hence we get an upper limit on λ_R^{11} . In the second case, there is a certain value of λ_R^{12} (within the perturbative regime) which nullifies the prefactor of λ_R^{11} ; hence that latter coupling can be arbitrarily large. This behaviour explains the shape of the allowed regions in the plot. The upper limit on λ_R^{11} can also be described by the formula

$$\lambda_R^{11} < \frac{2m_{S_1}^2 \sqrt{\omega_{\text{capt}} \text{BR}(\mu - e)}}{\alpha_s \lambda_L^{12} - \sqrt{4\pi} \alpha_v} \text{ if } \lambda_L^{12} > \frac{\alpha_v}{\alpha_s} \sqrt{4\pi}, \quad (48)$$

which is valid with $L \leftrightarrow R$ replacement and again explains the shape of the plot.

IX. CONCLUSIONS

In the present paper, we have analyzed the impact of combining Δa_μ with CLFV limits on the parameter space of the S_1 leptoquark model. This well-motivated model involves two 3×3 coupling matrices $\lambda_{L,R}^{q\ell}$ whose entries are strongly constrained by the combination of low-energy lepton observables. Here we briefly summarize and comment on the most important results.

The summary is also displayed in Table III in a matrix form, such that the $q\ell$ -entry of Table III collects constraints on the entries $\lambda_{L,R}^{q\ell}$.

Generally Δa_μ from equation (1) implies upper and lower limits on the left-right products of couplings to muons, and CLFV constraints then lead to upper limits on left-right products of couplings to the electron and τ lepton. In addition, perturbativity and the $K^+ \rightarrow \pi^+ \nu \bar{\nu}$ decay imply upper limits on individual couplings; these (together with limits on products) produce also lower limits on other individual couplings.

Specifically the third row of Table III assumes the ‘‘top-only’’ scenario (see section IV) where Δa_μ is explained via top-quark couplings only. In this case the (geometric average of left- and right-handed) couplings to electrons must be more than 4 orders of magnitude

$q \setminus \ell$	e	μ	τ	valid
u	$\lambda_L^{11} \lambda_R^{11} \lambda_L^{12} \lambda_R^{12} < 6.5 \cdot 10^{-12} \rightarrow 3.7 \cdot 10^{-14}$		—	any sc.
	$\lambda_L^{11} (\lambda_R^{12} - 0.65) < 2.9 \cdot 10^{-6} \rightarrow$ $\lambda_L^{11} (\lambda_R^{12} - 0.40) < 2.4 \cdot 10^{-7}$	$\lambda_L^{12} < 0.82$		
c	$\lambda_L^{21} \lambda_R^{21} < 1.2 \cdot 10^{-10} \rightarrow 1.8 \cdot 10^{-11}$	$0.18 < \lambda_L^{22} \lambda_R^{22} < 0.56$	$\lambda_L^{23} \lambda_R^{23} < 2.1 \cdot 10^{-2} \rightarrow 3.2 \cdot 10^{-3}$	sc. 2
	$\lambda_{L,R}^{21} < 1.3 \cdot 10^{-4} \rightarrow 5.0 \cdot 10^{-5}$	$5.1 \cdot 10^{-2} < \lambda_{L,R}^{22} < \sqrt{4\pi}$	$\lambda_{L,R}^{23} < 1.7 \rightarrow 0.67$	
	$\lambda_L^{21} < 4.6 \cdot 10^{-6} \rightarrow 1.7 \cdot 10^{-6}$	$\lambda_L^{22} < 0.13, 1.5 < \lambda_R^{22}$	$\lambda_L^{23} < 6.0 \cdot 10^{-2} \rightarrow 2.3 \cdot 10^{-2}$	
t	$\lambda_L^{31} \lambda_R^{31} < 2.1 \cdot 10^{-12} \rightarrow 2.9 \cdot 10^{-13}$	$3.1 \cdot 10^{-3} < \lambda_L^{32} \lambda_R^{32} < 9.3 \cdot 10^{-3}$	$\lambda_L^{33} \lambda_R^{33} < 3.5 \cdot 10^{-4} \rightarrow 5.4 \cdot 10^{-5}$	sc. 1
	$\lambda_{L,R}^{31} < 1.3 \cdot 10^{-4} \rightarrow 4.9 \cdot 10^{-5}$	$8.7 \cdot 10^{-4} < \lambda_{L,R}^{32} < \sqrt{4\pi}$	$\lambda_{L,R}^{33} < 1.7 \rightarrow 0.66$	

TABLE III: Summary of restrictions on all entries of the S_1 leptoquark coupling matrices $\lambda_{L,R}$ for $m_{S_1} = 1.8$ TeV. The restrictions in the second and third rows are valid under the condition that Δa_μ of equation (1) is explained, and they apply to various scenarios of Sec. IV as indicated in the rightmost columns. For the derivation and the range of validity of the constraints on individual couplings we refer to the appropriate sections and text.

smaller than the corresponding couplings to muons. Also, the couplings to τ leptons must be smaller than the couplings to muons. In the absence of cancellations within the theory predictions, this conclusion remains unchanged even in the more general case where couplings to the charm- and up-quarks are also allowed to be nonzero (but small so as to not significantly modify the contributions to Δa_μ).

Similarly, the second row of Table III assumes the “charm-only” scenario and presents bounds on couplings of leptons to the charm-quark. In order to accommodate the current Δa_μ value, the couplings to the muon must be $\mathcal{O}(1)$. In addition, the $K^+ \rightarrow \pi^+ \nu \bar{\nu}$ decay implies limits on the ratio of left- and right-handed couplings, valid in a wide range of parameter space (see section V for details). These are also reflected in the asymmetries visible in Figures 6b and 7b for the $\mu \rightarrow e \gamma$ and $\tau \rightarrow \mu \gamma$ decays. Again, there must be a strong hierarchy between charm-couplings to the muon and to the electron.

Finally, the first row of Table III is valid irrespective of the scenario. It is derived from $\mu \rightarrow e$ conversion constraints and from the $K^+ \rightarrow \pi^+ \nu \bar{\nu}$ decay. As a result of these constraints, the (geometric average of the) couplings of electrons and muons to the up-quark must be significantly smaller than the couplings to the charm- or top-quarks if the

Δa_μ deviation is accommodated. In addition, more detailed limits on λ_L^{12} and on products of two couplings can be given as shown in the Table III and as explained in section VIII.

The table also collects the possible improvements of limits from the next phases of CLFV experiments collected in Table I. If no signal is found, they will significantly sharpen the upper limits on couplings to electrons and τ leptons and will increase the need for highly hierarchical and non-universal entries in the coupling matrices $\lambda_{L,R}^{q\ell}$. In general, the results exemplify the implications of Δa_μ and CLFV constraints on the flavor structure of new physics models with enhanced chirality flips. Concrete models of flavor need to be compatible with such results. This is of particular interest in the considered case of leptoquarks, where an obvious and unambiguous notion of minimal flavor violation is not available [117, 118].

ACKNOWLEDGMENTS

U.Kh. was supported by the Deutscher Akademischer Austauschdienst (DAAD) under Research Grants — Doctoral Programmes in Germany, 2019/20 (57440921) and by the Deutsche Forschungsgemeinschaft (DFG) under grant number STO 876/7-1.

Appendix A: Constraints from flavor-conserving meson decays

In this appendix, we discuss the impact of two lepton flavor-conserving decays on the leptoquark parameter space. Both decays have been used in Ref. [50] to constrain the case of charmphilic explanations of Δa_μ . For earlier, original calculations and analyses of further meson decays within leptoquark models see Refs. [59, 66, 119]. Here we generalize the results of Ref. [50] to the case of general coupling structures.

1. Decay $K^+ \rightarrow \pi^+ \nu \bar{\nu}$

From Ref. [50] one obtains the following leptoquark contribution to the branching ratio

$$\text{BR}(K^+ \rightarrow \pi^+ \nu \bar{\nu})_{\text{LQ}} = k_1 C_{VLL}^{K1\ell} (C_{VLL}^{K1\ell} + k_2), \quad (\text{A1})$$

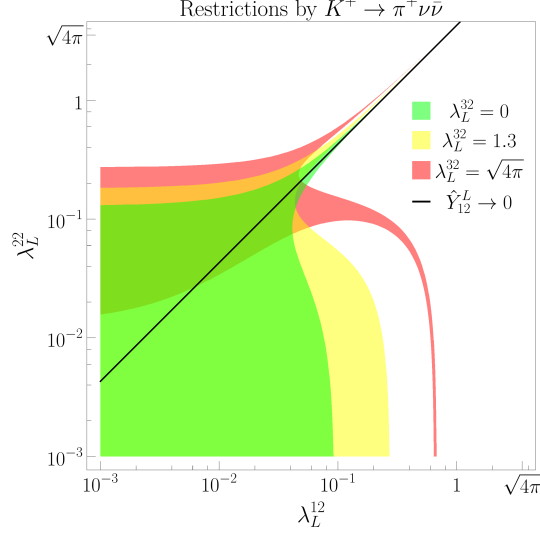


FIG. 10: Constraints from the $K^+ \rightarrow \pi^+ \nu \bar{\nu}$ decay in the $\lambda_L^{12}-\lambda_L^{22}$ plane, for different values of λ_L^{32} . The colored regions are allowed for the indicated values of λ_L^{32} .

where the following abbreviations are used

$$\begin{aligned}
C_{VLL}^{K1\ell} &= \frac{1}{2m_{S_1}^2} \hat{Y}_{12}^L \hat{Y}_{22}^{L*}, & \hat{Y}_{qt}^L &= V_{\text{CKM}}^{iq} \lambda_L^{il}, \\
k_1 &= \frac{\kappa_+}{3C_F^2 \lambda^{10}} \approx 1.83595 \cdot 10^9 \text{ GeV}^4, \\
k_2 &= 2C_F |\text{Re}[\lambda_t] X(m_t^2/m_W^2) + \lambda_c X_{NL}^e| \\
&\approx 2.65751 \cdot 10^{-10} \text{ GeV}^{-2}
\end{aligned} \tag{A2}$$

with the numerical values of intermediate parameters as in Ref. [50]; after subtracting the SM branching ratio ($\text{BR}(K^+ \rightarrow \pi^+ \nu \bar{\nu})_{\text{SM}} \approx 9 \cdot 10^{-11}$) from the experimental limit obtained by the E949 Collaboration [102] one obtains the following 2σ bounds:

$$-1.27 \cdot 10^{-10} < \text{BR}(K^+ \rightarrow \pi^+ \nu \bar{\nu})_{\text{LQ}} < 3.13 \cdot 10^{-10}. \tag{A3}$$

The $K^+ \rightarrow \pi^+ \nu \bar{\nu}$ decay thus constrains a combination of the three left-handed parameters λ_L^{i2} ($i = 1, 2, 3$). The numerical result is shown in Figure 10 in the plane of $\lambda_L^{12}-\lambda_L^{22}$ (λ_L^{32} is less important since it appears only multiplied with small CKM matrix elements).

The green area corresponds to the allowed region for the special case $\lambda_L^{32} = 0$. There is a thin allowed strip which is always allowed as \hat{Y}_{12}^L vanishes due to different signs of CKM matrix entries. This strip is cut off only by the perturbativity limit.

If λ_L^{32} is allowed to be nonzero, the allowed region in the $\lambda_L^{12}-\lambda_L^{22}$ plane can increase. The yellow area corresponds to the choice $\lambda_L^{32} = 1.3$. Here the allowed region has a similar shape

as the green region but extends to larger coupling values. If λ_L^{32} is increased further, the shape of the allowed region changes. The reason is that specific values of the up- and charm-quark-couplings are required to cancel the large top-coupling contributions. The red region illustrates this for the value of λ_L^{32} at the perturbativity limit. This region also illustrates the absolute achievable upper limit

$$\lambda_L^{12} < 0.82, \quad (\text{A4})$$

which is used in Figure 9b.

2. Decay $D^0 \rightarrow \mu^+ \mu^-$

The current experimental bound is the following [103]:

$$\text{BR}(D^0 \rightarrow \mu^+ \mu^-) < 7.6 \cdot 10^{-9} \text{ (95\% CL)}. \quad (\text{A5})$$

The expression for the branching ratio has the form:

$$\begin{aligned} \text{BR}(D^0 \rightarrow \mu^+ \mu^-) = \frac{d_1}{m_{S_1}^4} & \left[(\lambda_L^{12} \lambda_R^{22} - \lambda_R^{12} \lambda_L^{22})^2 \right. \\ & + (\lambda_L^{12} \lambda_R^{22} + \lambda_R^{12} \lambda_L^{22}) \\ & \left. + d_2 (\lambda_L^{12} \lambda_L^{22} + \lambda_R^{12} \lambda_R^{22}) \right]^2 \end{aligned} \quad (\text{A6})$$

with the following abbreviations and numerical values from [50]:

$$\begin{aligned} d_1 &= \tau_D \frac{f_D^2}{256\pi} \frac{m_D^5}{m_c^2} \approx (17.3 \text{ GeV})^4, \\ d_2 &= \frac{m_\mu m_c}{m_D} \approx 0.0391. \end{aligned} \quad (\text{A7})$$

This decay leads to relevant constraints for the down-type coupling basis considered in Ref. [50]. For our purposes, we employ the up-type basis and several scenarios as described in section IV. We have checked that for all our scenarios this decay does not lead to additional bounds on parameter space beyond the bounds presented in the main text of the paper.

[1] D. P. Aguillard *et al.* (Muon g-2), Measurement of the Positive Muon Anomalous Magnetic Moment to 0.20 ppm, (2023), arXiv:2308.06230 [hep-ex].

- [2] B. Abi *et al.* (Muon $g-2$), Measurement of the Positive Muon Anomalous Magnetic Moment to 0.46 ppm, *Phys. Rev. Lett.* **126**, 141801 (2021), arXiv:2104.03281 [hep-ex].
- [3] G. W. Bennett *et al.* (Muon $g-2$), Final Report of the Muon E821 Anomalous Magnetic Moment Measurement at BNL, *Phys. Rev. D* **73**, 072003 (2006), arXiv:hep-ex/0602035.
- [4] T. Aoyama *et al.*, The anomalous magnetic moment of the muon in the Standard Model, *Phys. Rept.* **887**, 1 (2020), arXiv:2006.04822 [hep-ph].
- [5] T. Aoyama, M. Hayakawa, T. Kinoshita, and M. Nio, Complete Tenth-Order QED Contribution to the Muon $g-2$, *Phys. Rev. Lett.* **109**, 111808 (2012), arXiv:1205.5370 [hep-ph].
- [6] T. Aoyama, T. Kinoshita, and M. Nio, Theory of the Anomalous Magnetic Moment of the Electron, *Atoms* **7**, 28 (2019).
- [7] A. Czarnecki, W. J. Marciano, and A. Vainshtein, Refinements in electroweak contributions to the muon anomalous magnetic moment, *Phys. Rev. D* **67**, 073006 (2003), [Erratum: *Phys.Rev.D* 73, 119901 (2006)], arXiv:hep-ph/0212229.
- [8] C. Gnendiger, D. Stöckinger, and H. Stöckinger-Kim, The electroweak contributions to $(g-2)_\mu$ after the Higgs boson mass measurement, *Phys. Rev. D* **88**, 053005 (2013), arXiv:1306.5546 [hep-ph].
- [9] M. Davier, A. Hoecker, B. Malaescu, and Z. Zhang, Reevaluation of the hadronic vacuum polarisation contributions to the Standard Model predictions of the muon $g-2$ and $\alpha(m_Z^2)$ using newest hadronic cross-section data, *Eur. Phys. J. C* **77**, 827 (2017), arXiv:1706.09436 [hep-ph].
- [10] A. Keshavarzi, D. Nomura, and T. Teubner, Muon $g-2$ and $\alpha(M_Z^2)$: a new data-based analysis, *Phys. Rev. D* **97**, 114025 (2018), arXiv:1802.02995 [hep-ph].
- [11] G. Colangelo, M. Hoferichter, and P. Stoffer, Two-pion contribution to hadronic vacuum polarization, *JHEP* **02**, 006, arXiv:1810.00007 [hep-ph].
- [12] M. Hoferichter, B.-L. Hoid, and B. Kubis, Three-pion contribution to hadronic vacuum polarization, *JHEP* **08**, 137, arXiv:1907.01556 [hep-ph].
- [13] M. Davier, A. Hoecker, B. Malaescu, and Z. Zhang, A new evaluation of the hadronic vacuum polarisation contributions to the muon anomalous magnetic moment and to $\alpha(m_Z^2)$, *Eur. Phys. J. C* **80**, 241 (2020), [Erratum: *Eur.Phys.J.C* 80, 410 (2020)], arXiv:1908.00921 [hep-ph].
- [14] A. Keshavarzi, D. Nomura, and T. Teubner, $g-2$ of charged leptons, $\alpha(M_Z^2)$, and the

- hyperfine splitting of muonium, Phys. Rev. D **101**, 014029 (2020), arXiv:1911.00367 [hep-ph].
- [15] A. Kurz, T. Liu, P. Marquard, and M. Steinhauser, Hadronic contribution to the muon anomalous magnetic moment to next-to-next-to-leading order, Phys. Lett. B **734**, 144 (2014), arXiv:1403.6400 [hep-ph].
- [16] K. Melnikov and A. Vainshtein, Hadronic light-by-light scattering contribution to the muon anomalous magnetic moment revisited, Phys. Rev. D **70**, 113006 (2004), arXiv:hep-ph/0312226.
- [17] P. Masjuan and P. Sanchez-Puertas, Pseudoscalar-pole contribution to the $(g_\mu - 2)$: a rational approach, Phys. Rev. D **95**, 054026 (2017), arXiv:1701.05829 [hep-ph].
- [18] G. Colangelo, M. Hoferichter, M. Procura, and P. Stoffer, Dispersion relation for hadronic light-by-light scattering: two-pion contributions, JHEP **04**, 161, arXiv:1702.07347 [hep-ph].
- [19] M. Hoferichter, B.-L. Hoid, B. Kubis, S. Leupold, and S. P. Schneider, Dispersion relation for hadronic light-by-light scattering: pion pole, JHEP **10**, 141, arXiv:1808.04823 [hep-ph].
- [20] A. Gérardin, H. B. Meyer, and A. Nyffeler, Lattice calculation of the pion transition form factor with $N_f = 2 + 1$ Wilson quarks, Phys. Rev. D **100**, 034520 (2019), arXiv:1903.09471 [hep-lat].
- [21] J. Bijnens, N. Hermansson-Truedsson, and A. Rodríguez-Sánchez, Short-distance constraints for the HLbL contribution to the muon anomalous magnetic moment, Phys. Lett. B **798**, 134994 (2019), arXiv:1908.03331 [hep-ph].
- [22] G. Colangelo, F. Hagelstein, M. Hoferichter, L. Laub, and P. Stoffer, Longitudinal short-distance constraints for the hadronic light-by-light contribution to $(g - 2)_\mu$ with large- N_c Regge models, JHEP **03**, 101, arXiv:1910.13432 [hep-ph].
- [23] V. Pauk and M. Vanderhaeghen, Single meson contributions to the muon's anomalous magnetic moment, Eur. Phys. J. C **74**, 3008 (2014), arXiv:1401.0832 [hep-ph].
- [24] I. Danilkin and M. Vanderhaeghen, Light-by-light scattering sum rules in light of new data, Phys. Rev. D **95**, 014019 (2017), arXiv:1611.04646 [hep-ph].
- [25] F. Jegerlehner, *The Anomalous Magnetic Moment of the Muon*, Vol. 274 (Springer, Cham, 2017).
- [26] M. Knecht, S. Narison, A. Rabemananjara, and D. Rabetiarivony, Scalar meson contributions to a μ from hadronic light-by-light scattering, Phys. Lett. B **787**, 111 (2018), arXiv:1808.03848

- [hep-ph].
- [27] G. Eichmann, C. S. Fischer, and R. Williams, Kaon-box contribution to the anomalous magnetic moment of the muon, *Phys. Rev. D* **101**, 054015 (2020), arXiv:1910.06795 [hep-ph].
- [28] P. Roig and P. Sanchez-Puertas, Axial-vector exchange contribution to the hadronic light-by-light piece of the muon anomalous magnetic moment, *Phys. Rev. D* **101**, 074019 (2020), arXiv:1910.02881 [hep-ph].
- [29] T. Blum, N. Christ, M. Hayakawa, T. Izubuchi, L. Jin, C. Jung, and C. Lehner, Hadronic Light-by-Light Scattering Contribution to the Muon Anomalous Magnetic Moment from Lattice QCD, *Phys. Rev. Lett.* **124**, 132002 (2020), arXiv:1911.08123 [hep-lat].
- [30] G. Colangelo, M. Hoferichter, A. Nyffeler, M. Passera, and P. Stoffer, Remarks on higher-order hadronic corrections to the muon $g-2$, *Phys. Lett. B* **735**, 90 (2014), arXiv:1403.7512 [hep-ph].
- [31] S. Borsanyi *et al.*, Leading hadronic contribution to the muon magnetic moment from lattice QCD, *Nature* **593**, 51 (2021), arXiv:2002.12347 [hep-lat].
- [32] M. Cè *et al.*, Window observable for the hadronic vacuum polarization contribution to the muon $g-2$ from lattice QCD, *Phys. Rev. D* **106**, 114502 (2022), arXiv:2206.06582 [hep-lat].
- [33] C. Alexandrou *et al.*, Lattice calculation of the short and intermediate time-distance hadronic vacuum polarization contributions to the muon magnetic moment using twisted-mass fermions, (2022), arXiv:2206.15084 [hep-lat].
- [34] T. Blum *et al.*, An update of Euclidean windows of the hadronic vacuum polarization, (2023), arXiv:2301.08696 [hep-lat].
- [35] F. V. Ignatov *et al.* (CMD-3), Measurement of the $e^+e^- \rightarrow \pi^+\pi^-$ cross section from threshold to 1.2 GeV with the CMD-3 detector, (2023), arXiv:2302.08834 [hep-ex].
- [36] G. Colangelo *et al.*, Prospects for precise predictions of a_μ in the Standard Model, (2022), arXiv:2203.15810 [hep-ph].
- [37] P. Athron, C. Balázs, D. H. J. Jacob, W. Kotlarski, D. Stöckinger, and H. Stöckinger-Kim, New physics explanations of a_μ in light of the FNAL muon $g-2$ measurement, *JHEP* **09**, 080, arXiv:2104.03691 [hep-ph].
- [38] A. Crivellin and M. Hoferichter, Consequences of chirally enhanced explanations of $(g-2)_\mu$ for $h \rightarrow \mu\mu$ and $Z \rightarrow \mu\mu$, *JHEP* **07**, 135, [Erratum: *JHEP* 10, 030 (2022)], arXiv:2104.03202 [hep-ph].

- [39] D. Stöckinger and H. Stöckinger-Kim, On the role of chirality flips for the muon magnetic moment and its relation to the muon mass, *Front. in Phys.* **10**, 944614 (2022).
- [40] R. Dermisek, K. Hermanek, N. McGinnis, and S. Yoon, Effective Field Theory of Chirally-Enhanced Muon Mass and Dipole Operators, (2023), arXiv:2302.14144 [hep-ph].
- [41] W. Buchmuller, R. Ruckl, and D. Wyler, Leptoquarks in Lepton - Quark Collisions, *Phys. Lett. B* **191**, 442 (1987), [Erratum: *Phys.Lett.B* 448, 320–320 (1999)].
- [42] D. Chakraverty, D. Choudhury, and A. Datta, A Nonsupersymmetric resolution of the anomalous muon magnetic moment, *Phys. Lett. B* **506**, 103 (2001), arXiv:hep-ph/0102180.
- [43] U. Mahanta, Implications of BNL measurement of delta a(mu) on a class of scalar leptoquark interactions, *Eur. Phys. J. C* **21**, 171 (2001), arXiv:hep-ph/0102176.
- [44] K.-m. Cheung, Muon anomalous magnetic moment and leptoquark solutions, *Phys. Rev. D* **64**, 033001 (2001), arXiv:hep-ph/0102238.
- [45] C. Biggio and M. Bordone, Minimal muon anomalous magnetic moment, *JHEP* **02**, 099, arXiv:1411.6799 [hep-ph].
- [46] M. Bauer and M. Neubert, Minimal Leptoquark Explanation for the $R_{D^{(*)}}$, R_K , and $(g-2)_\mu$ Anomalies, *Phys. Rev. Lett.* **116**, 141802 (2016), arXiv:1511.01900 [hep-ph].
- [47] O. Popov and G. A. White, One Leptoquark to unify them? Neutrino masses and unification in the light of $(g-2)_\mu$, $R_{D^{(*)}}$ and R_K anomalies, *Nucl. Phys. B* **923**, 324 (2017), arXiv:1611.04566 [hep-ph].
- [48] D. Das, C. Hati, G. Kumar, and N. Mahajan, Towards a unified explanation of $R_{D^{(*)}}$, R_K and $(g-2)_\mu$ anomalies in a left-right model with leptoquarks, *Phys. Rev. D* **94**, 055034 (2016), arXiv:1605.06313 [hep-ph].
- [49] E. Coluccio Leskow, G. D’Ambrosio, A. Crivellin, and D. Müller, $(g-2)_\mu$, lepton flavor violation, and Z decays with leptoquarks: Correlations and future prospects, *Phys. Rev. D* **95**, 055018 (2017), arXiv:1612.06858 [hep-ph].
- [50] K. Kowalska, E. M. Sessolo, and Y. Yamamoto, Constraints on charmphilic solutions to the muon $g-2$ with leptoquarks, *Phys. Rev. D* **99**, 055007 (2019), arXiv:1812.06851 [hep-ph].
- [51] I. Doršner, S. Fajfer, and O. Sumensari, Muon $g-2$ and scalar leptoquark mixing, *JHEP* **06**, 089, arXiv:1910.03877 [hep-ph].
- [52] A. Crivellin, D. Mueller, and F. Saturnino, Correlating $h \rightarrow \mu^+ \mu^-$ to the Anomalous Magnetic Moment of the Muon via Leptoquarks, *Phys. Rev. Lett.* **127**, 021801 (2021), arXiv:2008.02643

- [hep-ph].
- [53] V. Gherardi, D. Marzocca, and E. Venturini, Low-energy phenomenology of scalar leptoquarks at one-loop accuracy, *JHEP* **01**, 138, arXiv:2008.09548 [hep-ph].
 - [54] K. S. Babu, P. S. B. Dev, S. Jana, and A. Thapa, Unified framework for B -anomalies, muon $g - 2$ and neutrino masses, *JHEP* **03**, 179, arXiv:2009.01771 [hep-ph].
 - [55] A. Crivellin, C. Greub, D. Müller, and F. Saturnino, Scalar Leptoquarks in Leptonic Processes, *JHEP* **02**, 182, arXiv:2010.06593 [hep-ph].
 - [56] F. S. Queiroz and W. Shepherd, New Physics Contributions to the Muon Anomalous Magnetic Moment: A Numerical Code, *Phys. Rev. D* **89**, 095024 (2014), arXiv:1403.2309 [hep-ph].
 - [57] W.-C. Chiu, C.-Q. Geng, and D. Huang, Correlation Between Muon $g - 2$ and $\mu \rightarrow e\gamma$, *Phys. Rev. D* **91**, 013006 (2015), arXiv:1409.4198 [hep-ph].
 - [58] C. Biggio, M. Bordone, L. Di Luzio, and G. Ridolfi, Massive vectors and loop observables: the $g - 2$ case, *JHEP* **10**, 002, arXiv:1607.07621 [hep-ph].
 - [59] Y. Cai, J. Gargalionis, M. A. Schmidt, and R. R. Volkas, Reconsidering the One Leptoquark solution: flavor anomalies and neutrino mass, *JHEP* **10**, 047, arXiv:1704.05849 [hep-ph].
 - [60] A. Crivellin, D. Müller, and T. Ota, Simultaneous explanation of $R(D^{(*)})$ and $b \rightarrow s\mu^+\mu^-$: the last scalar leptoquarks standing, *JHEP* **09**, 040, arXiv:1703.09226 [hep-ph].
 - [61] T. Nomura and H. Okada, Explanations for anomalies of muon anomalous magnetic dipole moment, $b \rightarrow s\mu\mu^-$, and radiative neutrino masses in a leptoquark model, *Phys. Rev. D* **104**, 035042 (2021), arXiv:2104.03248 [hep-ph].
 - [62] D. Marzocca and S. Trifinopoulos, Minimal Explanation of Flavor Anomalies: B-Meson Decays, Muon Magnetic Moment, and the Cabibbo Angle, *Phys. Rev. Lett.* **127**, 061803 (2021), arXiv:2104.05730 [hep-ph].
 - [63] D. Zhang, Radiative neutrino masses, lepton flavor mixing and muon $g - 2$ in a leptoquark model, *JHEP* **07**, 069, arXiv:2105.08670 [hep-ph].
 - [64] S.-L. Chen, W.-w. Jiang, and Z.-K. Liu, Combined explanations of B-physics anomalies, $(g - 2)_{e,\mu}$ and neutrino masses by scalar leptoquarks, *Eur. Phys. J. C* **82**, 959 (2022), arXiv:2205.15794 [hep-ph].
 - [65] F. F. Freitas, J. a. Gonçalves, A. P. Morais, R. Pasechnik, and W. Porod, On interplay between flavour anomalies and neutrino properties, (2022), arXiv:2206.01674 [hep-ph].
 - [66] S. de Boer and G. Hiller, Flavor and new physics opportunities with rare charm decays into

- leptons, Phys. Rev. D **93**, 074001 (2016), arXiv:1510.00311 [hep-ph].
- [67] R. Mandal and A. Pich, Constraints on scalar leptoquarks from lepton and kaon physics, JHEP **12**, 089, arXiv:1908.11155 [hep-ph].
- [68] I. Bigaran and R. R. Volkas, Getting chirality right: Single scalar leptoquark solutions to the $(g-2)_{e,\mu}$ puzzle, Phys. Rev. D **102**, 075037 (2020), arXiv:2002.12544 [hep-ph].
- [69] I. Doršner, S. Fajfer, and S. Saad, $\mu \rightarrow e\gamma$ selecting scalar leptoquark solutions for the $(g-2)_{e,\mu}$ puzzles, Phys. Rev. D **102**, 075007 (2020), arXiv:2006.11624 [hep-ph].
- [70] R. L. Workman *et al.* (Particle Data Group), Review of Particle Physics, PTEP **2022**, 083C01 (2022).
- [71] P. Athron, A. Büchner, D. Harries, W. Kotlarski, D. Stöckinger, and A. Voigt, FlexibleDecay: An automated calculator of scalar decay widths, (2021), arXiv:2106.05038 [hep-ph].
- [72] P. Athron, J.-h. Park, D. Stöckinger, and A. Voigt, FlexibleSUSY — A spectrum generator for supersymmetric models, Comput. Phys. Commun. **190**, 139 (2015), arXiv:1406.2319 [hep-ph].
- [73] P. Athron, M. Bach, D. Harries, T. Kwasnitza, J.-h. Park, D. Stöckinger, A. Voigt, and J. Ziebell, FlexibleSUSY 2.0: Extensions to investigate the phenomenology of SUSY and non-SUSY models, Comput. Phys. Commun. **230**, 145 (2018), arXiv:1710.03760 [hep-ph].
- [74] U. Khasianevich, W. Kotlarski, and D. Stöckinger, NPointFunctions: a calculator of amplitudes and observables in FlexibleSUSY, PoS **CompTools2021**, 036 (2022), arXiv:2206.00745 [hep-ph].
- [75] F. Staub, Exploring new models in all detail with SARAH, Adv. High Energy Phys. **2015**, 840780 (2015), arXiv:1503.04200 [hep-ph].
- [76] A. Vicente, Computer tools in particle physics, (2015), arXiv:1507.06349 [hep-ph].
- [77] G. Degrandi and G. F. Giudice, QED logarithms in the electroweak corrections to the muon anomalous magnetic moment, Phys. Rev. D **58**, 053007 (1998), arXiv:hep-ph/9803384.
- [78] P. von Weitershausen, M. Schafer, H. Stockinger-Kim, and D. Stockinger, Photonic SUSY Two-Loop Corrections to the Muon Magnetic Moment, Phys. Rev. D **81**, 093004 (2010), arXiv:1003.5820 [hep-ph].
- [79] J. Hisano, T. Moroi, K. Tobe, and M. Yamaguchi, Lepton flavor violation via right-handed neutrino Yukawa couplings in supersymmetric standard model, Phys. Rev. D **53**, 2442 (1996), arXiv:hep-ph/9510309.

- [80] W. Kotlarski, D. Stöckinger, and H. Stöckinger-Kim, Low-energy lepton physics in the MRSSM: $(g-2)_\mu$, $\mu \rightarrow e\gamma$ and $\mu \rightarrow e$ conversion, JHEP **08**, 082, arXiv:1902.06650 [hep-ph].
- [81] V. Dūdėnas, T. Gajdosik, U. Khasianevich, W. Kotlarski, and D. Stöckinger, Charged lepton flavor violating processes in the Grimus-Neufeld model, JHEP **09**, 174, arXiv:2206.00661 [hep-ph].
- [82] P. A. Zyla *et al.* (Particle Data Group), Review of Particle Physics, PTEP **2020**, 083C01 (2020).
- [83] A. M. Baldini *et al.* (MEG), Search for lepton flavour violating muon decay mediated by a new light particle in the MEG experiment, Eur. Phys. J. C **80**, 858 (2020), arXiv:2005.00339 [hep-ex].
- [84] B. Aubert *et al.* (BaBar), Searches for Lepton Flavor Violation in the Decays $\tau^\pm \rightarrow e^\pm \gamma$ and $\tau^\pm \rightarrow \mu^\pm \gamma$, Phys. Rev. Lett. **104**, 021802 (2010), arXiv:0908.2381 [hep-ex].
- [85] A. M. Baldini *et al.* (MEG II), The design of the MEG II experiment, Eur. Phys. J. C **78**, 380 (2018), arXiv:1801.04688 [physics.ins-det].
- [86] S. Banerjee *et al.*, Snowmass 2021 White Paper: Charged lepton flavor violation in the tau sector, (2022), arXiv:2203.14919 [hep-ph].
- [87] Y. Okada, K.-i. Okumura, and Y. Shimizu, $\mu \rightarrow e\gamma$ and $\mu \rightarrow 3e$ processes with polarized muons and supersymmetric grand unified theories, Phys. Rev. D **61**, 094001 (2000), arXiv:hep-ph/9906446.
- [88] A. Crivellin, S. Davidson, G. M. Pruna, and A. Signer, Renormalisation-group improved analysis of $\mu \rightarrow e$ processes in a systematic effective-field-theory approach, JHEP **05**, 117, arXiv:1702.03020 [hep-ph].
- [89] Y. Kuno and Y. Okada, Muon decay and physics beyond the standard model, Rev. Mod. Phys. **73**, 151 (2001), arXiv:hep-ph/9909265.
- [90] A. Ilakovac and A. Pilaftsis, Flavor violating charged lepton decays in seesaw-type models, Nucl. Phys. B **437**, 491 (1995), arXiv:hep-ph/9403398.
- [91] G. Passarino and M. J. G. Veltman, One Loop Corrections for e^+e^- Annihilation Into $\mu^+\mu^-$ in the Weinberg Model, Nucl. Phys. B **160**, 151 (1979).
- [92] U. Bellgardt *et al.* (SINDRUM), Search for the decay $\mu^+ \rightarrow e^+e^+e^-$, Nucl. Phys. B **299**, 1 (1988).
- [93] K. Arndt *et al.* (Mu3e), Technical design of the phase I Mu3e experiment, Nucl. Instrum.

- Meth. A **1014**, 165679 (2021), arXiv:2009.11690 [physics.ins-det].
- [94] R. Kitano, M. Koike, and Y. Okada, Detailed calculation of lepton flavor violating muon electron conversion rate for various nuclei, Phys. Rev. D **66**, 096002 (2002), [Erratum: Phys.Rev.D 76, 059902 (2007)], arXiv:hep-ph/0203110.
- [95] M. Hoferichter, J. Ruiz de Elvira, B. Kubis, and U.-G. Meißner, High-Precision Determination of the Pion-Nucleon σ Term from Roy-Steiner Equations, Phys. Rev. Lett. **115**, 092301 (2015), arXiv:1506.04142 [hep-ph].
- [96] R. H. Bernstein (Mu2e), The Mu2e Experiment, Front. in Phys. **7**, 1 (2019), arXiv:1901.11099 [physics.ins-det].
- [97] L. Allwicher, P. Arnan, D. Barducci, and M. Nardecchia, Perturbative unitarity constraints on generic Yukawa interactions, JHEP **10**, 129, arXiv:2108.00013 [hep-ph].
- [98] P. Bandyopadhyay, S. Jangid, and A. Karan, Constraining scalar doublet and triplet leptoquarks with vacuum stability and perturbativity, Eur. Phys. J. C **82**, 516 (2022), arXiv:2111.03872 [hep-ph].
- [99] K. Hayasaka *et al.*, Search for lepton flavor violating τ decays into three leptons with 719 million produced $\tau^+\tau^-$ Pairs, Phys. Lett. B **687**, 139 (2010), arXiv:1001.3221 [hep-ex].
- [100] W. H. Bertl *et al.* (SINDRUM II), A Search for muon to electron conversion in muonic gold, Eur. Phys. J. C **47**, 337 (2006).
- [101] R. Abramishvili *et al.* (COMET), COMET Phase-I Technical Design Report, PTEP **2020**, 033C01 (2020), arXiv:1812.09018 [physics.ins-det].
- [102] A. V. Artamonov *et al.* (E949), New measurement of the $K^+ \rightarrow \pi^+ \nu \bar{\nu}$ branching ratio, Phys. Rev. Lett. **101**, 191802 (2008), arXiv:0808.2459 [hep-ex].
- [103] R. Aaij *et al.* (LHCb), Search for the rare decay $D^0 \rightarrow \mu^+ \mu^-$, Phys. Lett. B **725**, 15 (2013), arXiv:1305.5059 [hep-ex].
- [104] A. M. Sirunyan *et al.* (CMS), Search for pair production of first-generation scalar leptoquarks at $\sqrt{s} = 13$ TeV, Phys. Rev. D **99**, 052002 (2019), arXiv:1811.01197 [hep-ex].
- [105] M. Aaboud *et al.* (ATLAS), Searches for scalar leptoquarks and differential cross-section measurements in dilepton-dijet events in proton-proton collisions at a centre-of-mass energy of $\sqrt{s} = 13$ TeV with the ATLAS experiment, Eur. Phys. J. C **79**, 733 (2019), arXiv:1902.00377 [hep-ex].
- [106] V. Khachatryan *et al.* (CMS), Search for single production of scalar leptoquarks in proton-

- proton collisions at $\sqrt{s} = 8 \text{ TeV}$, Phys. Rev. D **93**, 032005 (2016), [Erratum: Phys.Rev.D 95, 039906 (2017)], arXiv:1509.03750 [hep-ex].
- [107] A. M. Sirunyan *et al.* (CMS), Search for pair production of second-generation leptoquarks at $\sqrt{s} = 13 \text{ TeV}$, Phys. Rev. D **99**, 032014 (2019), arXiv:1808.05082 [hep-ex].
- [108] A. M. Sirunyan *et al.* (CMS), Search for leptoquarks coupled to third-generation quarks in proton-proton collisions at $\sqrt{s} = 13 \text{ TeV}$, Phys. Rev. Lett. **121**, 241802 (2018), arXiv:1809.05558 [hep-ex].
- [109] A. M. Sirunyan *et al.* (CMS), Search for singly and pair-produced leptoquarks coupling to third-generation fermions in proton-proton collisions at $s=13 \text{ TeV}$, Phys. Lett. B **819**, 136446 (2021), arXiv:2012.04178 [hep-ex].
- [110] M. Aaboud *et al.* (ATLAS), Searches for third-generation scalar leptoquarks in $\sqrt{s} = 13 \text{ TeV}$ pp collisions with the ATLAS detector, JHEP **06**, 144, arXiv:1902.08103 [hep-ex].
- [111] N. Raj, Anticipating nonresonant new physics in dilepton angular spectra at the LHC, Phys. Rev. D **95**, 015011 (2017), arXiv:1610.03795 [hep-ph].
- [112] S. Bansal, R. M. Capdevilla, A. Delgado, C. Kolda, A. Martin, and N. Raj, Hunting leptoquarks in monolepton searches, Phys. Rev. D **98**, 015037 (2018), arXiv:1806.02370 [hep-ph].
- [113] J. Fuentes-Martin, A. Greljo, J. Martin Camalich, and J. D. Ruiz-Alvarez, Charm physics confronts high- p_T lepton tails, JHEP **11**, 080, arXiv:2003.12421 [hep-ph].
- [114] I. Bigaran and R. R. Volkas, Reflecting on chirality: CP-violating extensions of the single scalar-leptoquark solutions for the $(g-2)_{e,\mu}$ puzzles and their implications for lepton EDMs, Phys. Rev. D **105**, 015002 (2022), arXiv:2110.03707 [hep-ph].
- [115] J. Abdallah *et al.* (DELPHI), Study of tau-pair production in photon-photon collisions at LEP and limits on the anomalous electromagnetic moments of the tau lepton, Eur. Phys. J. C **35**, 159 (2004), arXiv:hep-ex/0406010.
- [116] N. Burmasov, E. Kryshen, P. Buehler, and R. Lavicka, Feasibility of tau $g-2$ measurements in ultra-peripheral collisions of heavy ions, in *16th International Workshop on Tau Lepton Physics* (2022) arXiv:2203.00990 [hep-ph].
- [117] S. Davidson and F. Palorini, Various definitions of Minimal Flavour Violation for Leptons, Phys. Lett. B **642**, 72 (2006), arXiv:hep-ph/0607329.
- [118] S. Davidson and S. Descotes-Genon, Minimal Flavour Violation for Leptoquarks, JHEP **11**, 073, arXiv:1009.1998 [hep-ph].

- [119] S. Fajfer and N. Košnik, Prospects of discovering new physics in rare charm decays, *Eur. Phys. J. C* **75**, 567 (2015), arXiv:1510.00965 [hep-ph].